Chapter 11B. Analysis of Imaging Spectrometer Data for the Nalbandon Area of Interest

By Trude V.V. King

Abstract

Computer analysis of the HyMap spectroscopic data of the Nalbandon area of interest (AOI) in the west-central part of Afghanistan used spectrum matching techniques to identify the occurrence of selected materials at the surface based on characteristic absorption features (absorption bands) in the HyMap data compared to a library of spectral standards. Carbonate minerals dominate the large Nalbandon AOI as well as the Nalbandon District and Gharghanaw-Gawmazar subarea. Iron oxides and hydroxides are present throughout the AOI with Fe^{2+} minerals dominating in the Proterozoic rocks north of the Hari Rud fault zone. Bedding planes consisting of assemblages of iron-bearing minerals and goethites can be traced for tens of kilometers across the AOI. The known mineral occurrences in the Gharghanaw-Gawmazar subarea seemingly correspond to areas containing Fe^{3+}, iron hydroxide, and goethitic minerals. The majority of the known lead-zinc and polymetallic-vein occurrences in the Nalbandon District are not associated with any particular mineral or group of minerals, with the exception of the Minora and Zawar polymetallic occurrences, which show an affinity with hematitic minerals. The only occurrence of groups of minerals associated with epithermal deposits (alunite, kaolinite, jarosite, pyrophyllite, and hydrated silica) is in the most northern part of the Nalbandon District (north and east of the Minora known mineral occurrence). The horizontally bedded rock units (little horizontal surface expression), the alteration mineral assemblages and patterns associated with lead-zinc deposits, and the presence of abundant dry vegetation, which may have masked the surficial minerals in a significant and geologically important part of the area, have reduced the utility of the imaging spectrometer data for overall site characterization in the Nalbandon AOI.

11B.1 Introduction

Previous U.S. Geological Survey (USGS) analyses of existing geologic data of Afghanistan revealed numerous areas with indications of potential mineral resources of various types (Peters and others, 2007). From these areas of interest, several were selected for follow-on studies using modern imaging spectrometer remote sensing data to further characterize surface materials. One of those areas is the Nalbandon area in west-central Afghanistan.

The Nalbandon area is about 460 kilometers (km) west and south of Kabul (fig. 11B–1) and is believed to have the potential for sandstone-hosted lead-zinc, Phanerozoic sedex zinc, lead-silver-gold, Mississippi Valley-type lead-zinc, and bedded barite deposits. To help assess these potential resources, high-resolution imaging spectrometer data were analyzed to detect the presence of selected minerals that may be indicative of past mineralization processes. This report contains the results of those analyses and identifies numerous sites with the Nalbandon area that could merit further investigation, especially detailed geological mapping and geochemical studies.

11B.1.1 Imaging Spectrometer Data Collection and Processing

In 2007, imaging spectrometer remote sensing data were acquired over most of Afghanistan with the HyMap imaging spectrometer (Cocks and others, 1998), as part of the USGS project "Oil and Gas Resources Assessment of the Katawaz and Helmand Basins" (Kokaly and others, 2008). These data were acquired from August 22 to October 2, 2007. There were 207 north-south flight lines and

11 cross-cutting calibration lines collected over Afghanistan for a total of 218 flight lines covering a surface area of 438,012 square kilometers (km^2) (Kokaly and others, 2008). These data provide a means for characterizing surface materials in support of assessments of resources (coal, water, minerals, and oil and gas) and earthquake hazards in the country. Imaging spectrometers measure the reflectance of visible and near-infrared light from the Earth's surface in many narrow channels, producing a reflectance spectrum for each image pixel. These reflectance spectra can be interpreted to identify specific chemical transitions and molecular bonds that provide compositional information about specific materials occurring at the surface. The imaging spectrometer sensor data can only be used to characterize the upper surface materials and not subsurface composition or structure.

After undergoing a complex and rigorous data calibration process, the georeferenced and calibrated reflectance data were processed. The reflectance spectrum of each pixel of HyMap data was compared to the spectral features of reference entries in a spectral library of minerals, vegetation, water, and other materials (King and others, 2011b; Kokaly and others, 2011). The best spectral matches were determined, and the results were clustered into classes of materials discussed below.

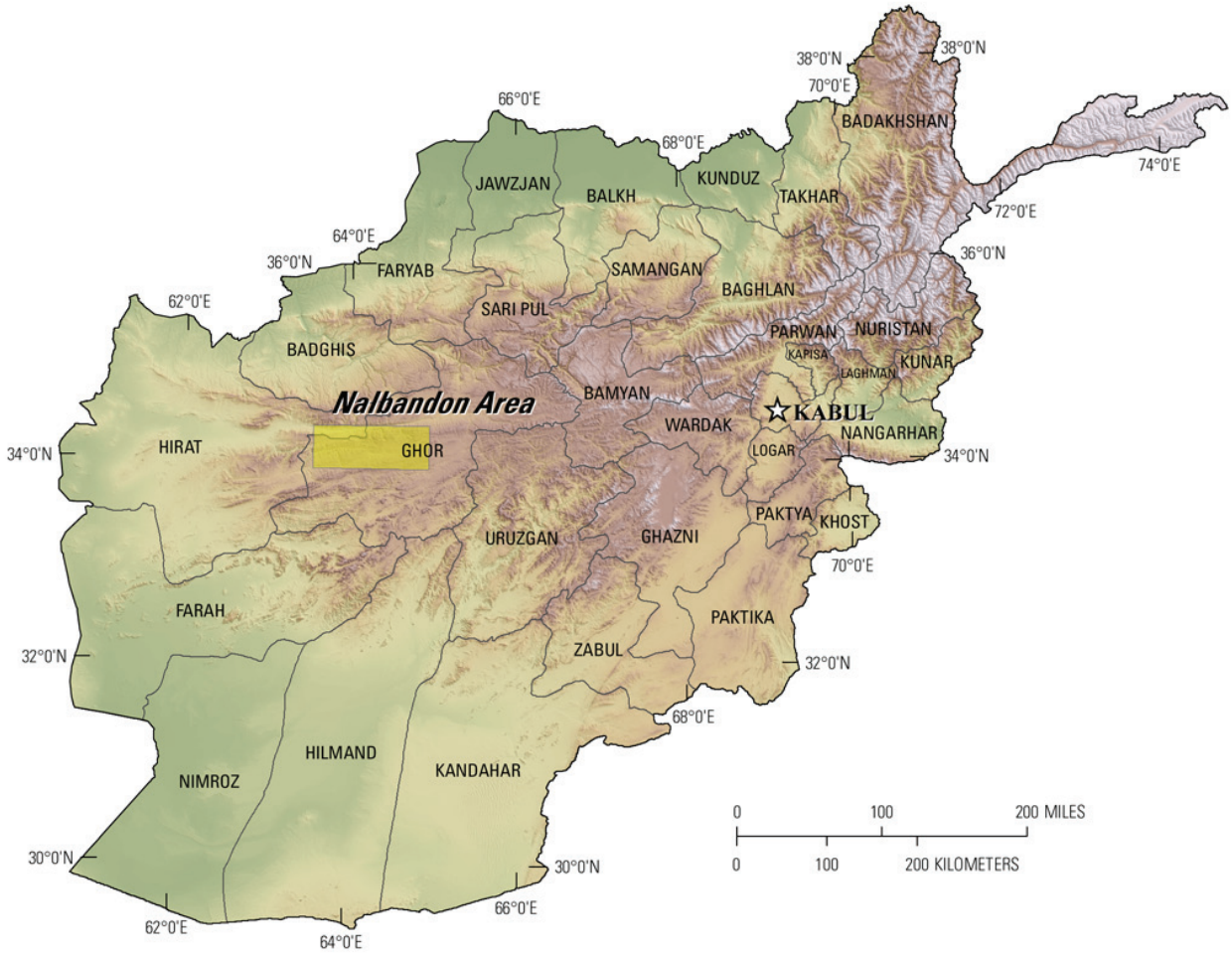

Figure 11B–1. The Nalbandon area of interest is located about 460 kilometers west and south of Kabul in the Ghor and Herat Provinces of Afghanistan.

11B.1.2 Calibration

To ensure the utility of the imaging spectrometer dataset, a rigorous calibration process to remove atmospheric absorptions and residual instrument artifacts was applied. Before the calibration process started, each flight line was georeferenced to Landsat base imagery in UTM projection (Davis, 2007). Because of the extreme topographic relief and restricted access to ground calibration sites,

modifications to the traditional USGS calibration procedures were required to calibrate the 2007 Afghanistan HyMap dataset (Hoefen and others, 2010). Radiance data were converted to apparent surface reflectance using the radiative transfer correction program Atmospheric CORrection Now (ACORN; ImSpec LLC, Palmdale, Calif.). ACORN was run multiple times for each flight line, using average elevations in 100-m increments covering the range of minimum to maximum elevation within the flight line. A single atmospherically corrected dataset was assembled from the ACORN results in 100-m increments. This was done by determining the elevation of each pixel and selecting the atmospherically corrected pixel from the 100-m increment closest to the elevation of the pixel. The atmospherically corrected dataset was further empirically adjusted using ground-based reflectance measurements from the Kandahar Air Field, Bagram Air Base, and Mazar-e-Sharif Airport, as well as soil samples from two fallow fields. To improve the data quality, new calibration techniques were developed to address the atmospheric differences within a flight line.

To refine data quality of ground-calibrated reflectance, a multiplier correction, computed by cross-calibrating north-south flight lines with a flight line that passes over a ground calibration site, was applied. For each north-south flight line, the pixels in overlap regions of north-south and cross-cutting calibration lines, subject to slope, vegetation cover, and other restrictions, were used to develop these cross-calibration correction factors (Hoefen and others, 2010). The cross-calibration multiplier corrected any residual atmospheric contamination in the imaging spectrometer data that was not present in the spectra of the ground calibration site.

11B.1.3 Materials Maps and Presentation

HyMap reflectance data were processed using MICA (Material Identification and Characterization Algorithm), a module of the USGS PRISM (Processing Routines in IDL for Spectroscopic Measurements) software (Kokaly, 2011). MICA compared the reflectance spectrum of each pixel of HyMap data entries in a reference spectral library of minerals, vegetation, water, and other materials. The HyMap data were compared to 97 reference spectra of well-characterized mineral and material standards. The resulting maps of material distribution, resampled to 23×23-square-meter (m^2) pixel grid, were used to prepare maps of mineral, vegetation, and other material occurrences.

HyMap data were analyzed twice. MICA was run using the set of minerals with absorption features in the visible and near-infrared wavelength region producing a 1-micrometer (μm) map of iron-bearing minerals and other materials (King and others, 2011b), and again using the minerals with absorption features in the shortwave infrared producing a 2-μm map of carbonates, phyllosilicates, sulfates, altered minerals, and other materials. For clarity of presentation, some individual classes in these two maps were bundled by combining selected specific mineral types (for example, kaolinites, montmorillonites, and hematites) to reduce the number of mineral classes. The iron-bearing minerals map has 27 classes. Iron-bearing minerals with different mineral compositions but similar spectral features are difficult to classify as specific mineral species. Thus, generic spectral classes, including several minerals with similar absorption features, such as Fe^{3+} type 1 and Fe^{3+} type 2 are depicted on the map. The carbonates, phyllosilicates, sulfates, and altered minerals map has 31 classes. Minerals with slightly different mineral compositions but similar spectral features are less easily discriminated; thus, some identified classes consist of several minerals with similar spectra, such as the chlorite or epidote class. When comparisons with reference spectra have no viable match, a designation of "not classified" was assigned to a pixel.

Although the occurrence of certain minerals (pyrophyllite, buddingtonite, dickite, and jarosite) may suggest that mineralization processes may have once operated in the area, many of the minerals that were identified are also common rock-forming minerals. Consequently, the distribution patterns of the identified minerals are extremely important in understanding the causes of mapped mineral occurrences and evaluating the possible potential for related mineral deposits.

11B.2 Geologic Setting of the Nalbandon Area

The main Nalbandon lead-zinc area is located in the Ghor and Herat Provinces of Afghanistan (fig. 11B–1). The main Nalbandon lead-zinc area is 6,150.55 km^2, and within this area of interest (AOI) lies the subareas of Nalbandon District (554 km^2) and Gharghanaw-Gawmazar (385 km^2). The elevation in the AOI ranges from 1,435 to 3,488 meters (m) (fig. 11B–2). The area is cut by two rivers that flow east-west. Numerous faults and fractures of different orientations and extent occur in the area (fig. 11B–3). Within the Nalbandon area, the prominent faults strike southwest to northeast. Known mineral occurrences commonly occur along the fracture systems.

11B.2.1 Lithology and Structure

The Nalbandon AOI has stratified rocks that range in age from Paleoproterozoic to Holocene and intrusive rocks of Mississippian, Late Triassic, Early Cretaceous, and Oligocene age (fig. 11B–4). A series of intrusive rocks are exposed in the northern part of the AOI along the Hari-Rud fracture zone.

11B.2.2 Known Mineralization

Figure 11B–5 shows 16 locations where reconnaissance field geology and geologic literature identified mineralization that suggests a potential for mineral resources. The mineralogical characteristics of the mineralized locations are summarized in Table 11B–1. These mineralization occurrences are of two types: (1) polymetallic veins and (2) Mississippi Valley-type lead-zinc deposits. Many of the noted mineral occurrences are relatively small and are at or below the spatial resolution of the HyMap data.

The geology of the Nalbandon area was first investigated by the German Geological Mission in 1963. The mineralization is located on the northern flank of the large syncline striking west-east (Peters and others, 2007).

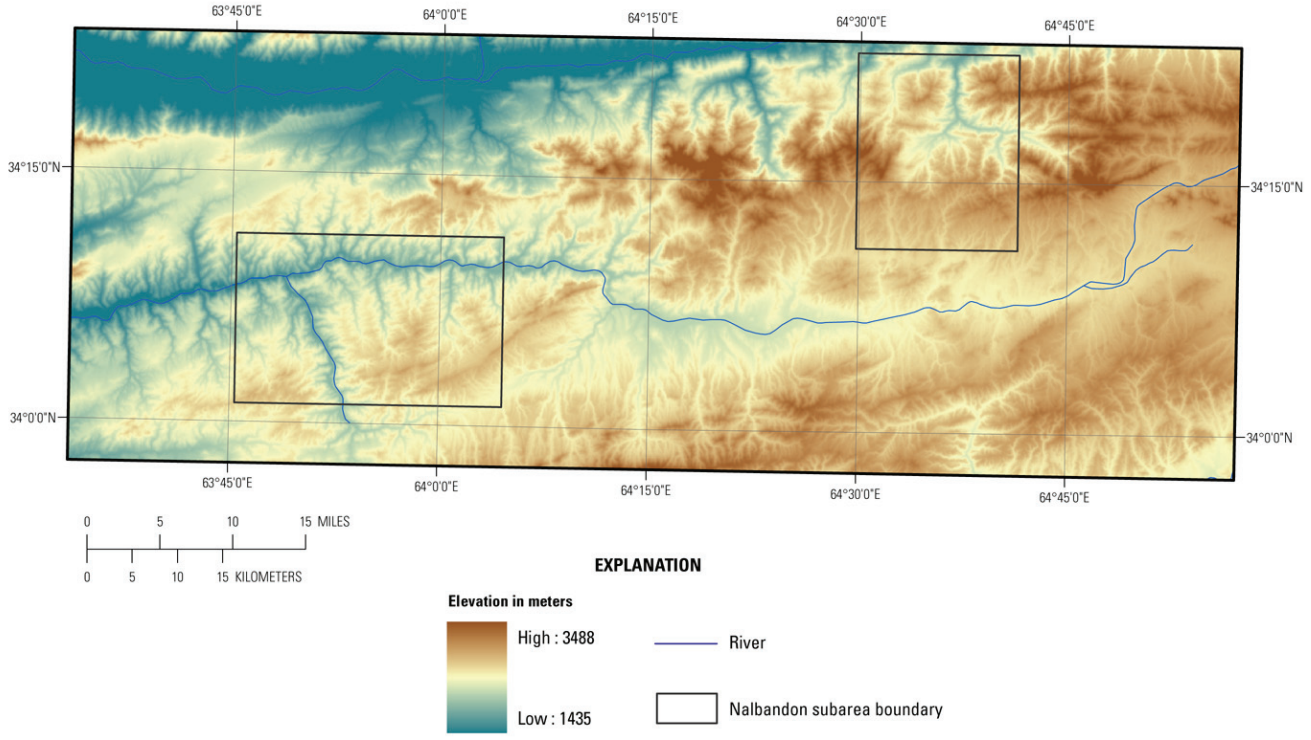

Figure 11B–2. Shaded relief map showing range of elevations in the Nalbandon area of interest.

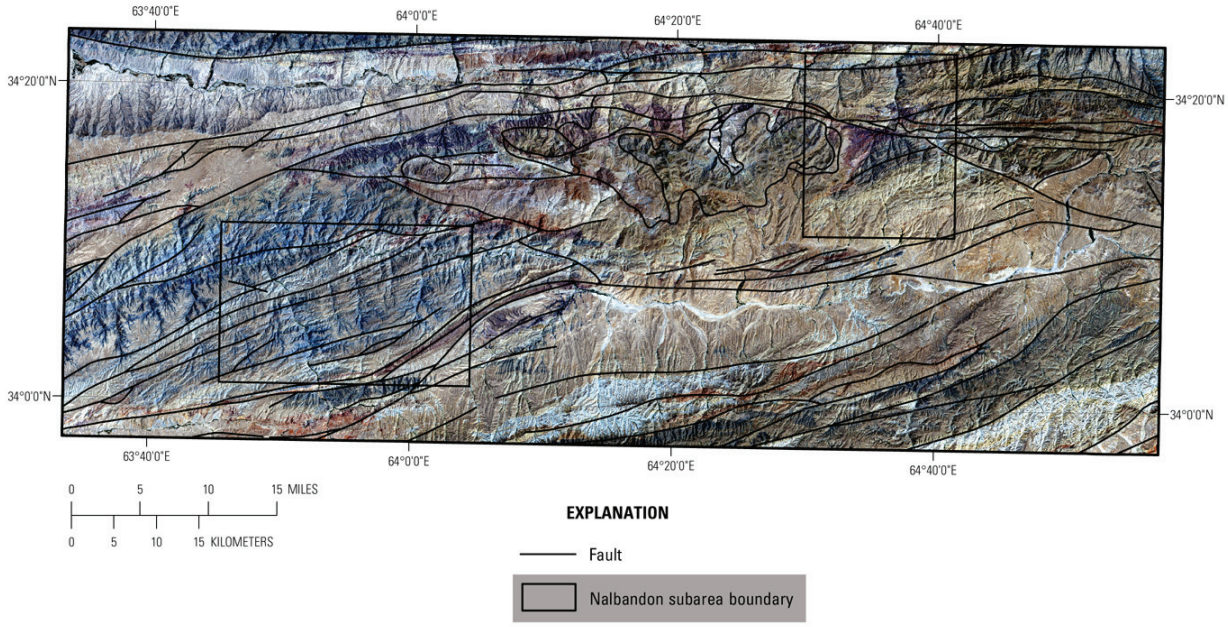

Figure 11B–3. Numerous faults and fractures of different orientations and extent occur within the Nalbandon area of interest. The fault traces (Peters and others, 2007) are placed on Landsat TM images (Davis, 2007).

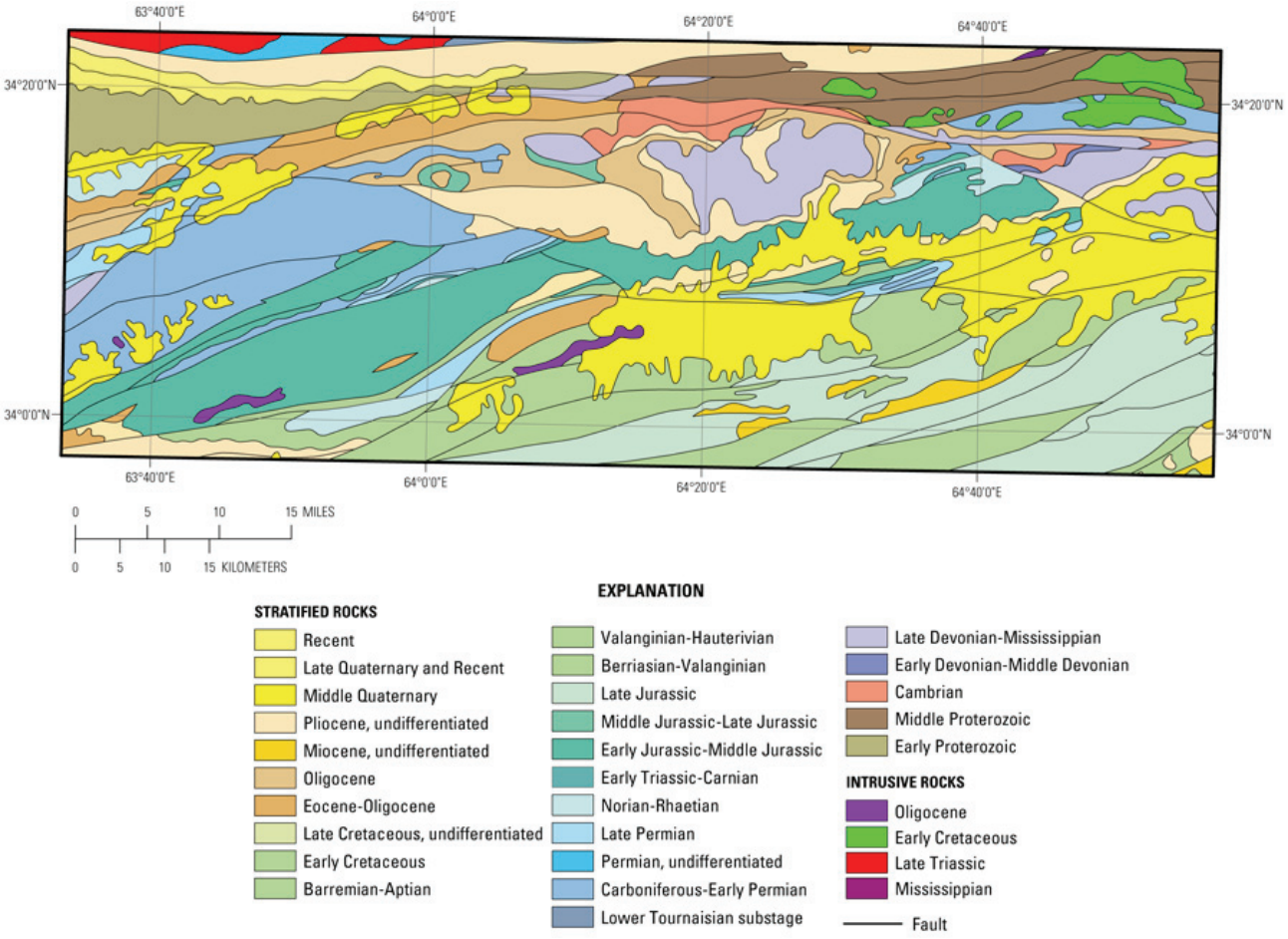

Figure 11B–4. Geologic map of the Nalbandon area of interest, from Doebrich and others (2006).

In the Nalbandon District, the lead-zinc occurrences are associated with shear zones and faults (Peters and others, 2007) . The Sarghul lead-zinc occurrence is within Lower to Middle Jurassic limestone and contains galena and sphalerite within sandstone lenses, accompanied by chalcopyrite and pyrrhotite (German Geological Mission, unpub. data, 1969). The Minora II polymetallic vein is in Triassic porous siltstone along a fault zone containing ferruginous quartz veins with traces of zinc and copper (Dronov and others, 1972). The Palang-Khana polymetallic occurrence is hosted in Lower to Middle Jurassic shale within two brecciated ferruginous zones containing silica veinlets and sparse galena.

The Gharghanaw-Gawmazar subarea is located in the northern part of the Nalbandon AOI. The Gharghanaw I and II lead-zinc mineral occurrences are hosted in lower Middle Jurassic sedimentary rocks within bedding-plane shear zones and contain zinc and traces of copper (Dronov and others, 1972). The Hasan-Sansalaghay lead-zinc occurrence is in a shear zone within Lower to Middle Jurassic sandstone and limestone (Dronov and others, 1972) and contains lead, zinc, copper, and traces of antimony. The Gawmazar I and II polymetallic deposits occur in silicified and carbonated, ferruginous shear zones in Upper Triassic sandy slate rocks that reportedly contain copper and gold. The Gawamazar III polymetallic-vein occurrence is in Upper Permian slaty sandstone in a wide shear zone that contains lead and minor zinc.

Table 11B–1. Deposit name, deposit type, mineralogy, and alteration of the known sites of mineralization in the Nalbandon area of interest.

Name	Deposit type	Mineralogy	Alteration
Kajnaw	Vein hematite	Hematite; limonite	
Zawar	Polymetallic vein	Chalcopyrite; galena; malachite	Silicification
Minora	Polymetallic vein	Sulfides; secondary mineral of cooper	Oxidation; silicification
Unnamed	Polymetallic vein	Sulfides	Silicification; carbonatization
Nalbandon	Mississippi Valley Zn-Pb	Sphalerite; galena; pyrite; chalcopyrite; boulangerite	
Ustoowa	Polymetallic vein	Galena; limonite	Limonitization; quartz alteration
Gawmazar IV	Polymetallic vein	Limonite	Silicification; limonitization
Gawmazar I & II	Polymetallic vein	Limonite	Silicification; carbonatization; limonitization
Gawmazar III	Polymetallic vein	No data	Silicification
Shekhlawast	Polymetallic vein	No data	Silicification
Hasan Sansalaghay	Mississippi Valley Zn-Pb	No data	
Gharghanaw II & III	Mississippi Valley Zn-Pb	Galena	Silicification
Minora II	Polymetallic vein	Limonite;	Silicification; limonitization
Palang-Khana	Polymetallic vein	Galena	Quartz alteration
Sarghul	Mississippi Valley Zn-Pb	Galena; sphalerite; chalcopyrite; boulangerite	
Tilak	Unknown Hg	Cinnabar	Carbonatization; dickitization

11B.3 Imaging Spectrometer Material Maps of the Nalbandon Area

Computer analysis of the HyMap data of the Nalbandon AOI using spectral mapping techniques resulted in the identification of a variety of surficial minerals. These minerals have been identified on the presence and wavelength position of absorption features in the 0.45–2.48 μm wavelength region. Two general categories of minerals are recognized: (1) iron-bearing minerals that have characteristic spectral absorption features that occur at wavelengths near the 1-μm region, and (2) a wide variety of minerals, including carbonates, mica and clay minerals, and sulfates, that have diagnostic spectral absorptions near the 2-μm region. Although the occurrence of certain minerals suggest mineralization processes may have operated in the area, many of the minerals identified and mapped are also common rock-forming minerals or minerals that can be derived from the weathering of a variety of rock types. Consequently, the distribution patterns of the identified minerals and the rocks where they occur are

extremely important in understanding the causes of the mapped mineral occurrences and assessing the possible potential for related mineral deposits.

Two general types of maps are included: (1) complete AOI maps showing the entire mapped suite of minerals that have absorption in the 1- and 2-µm-wavelength regions, and (2) topical maps that are subsets of the complete AOI maps. The topical maps, which depict selected groups of minerals that are mineralogically related or commonly occur together, are presented to show subtleties in the mineral distribution (figs. 11B–6 to 11B–12). A set of maps has been produced for the full Nalbandon AOI and each of the Nalbandon District and Gharghanaw-Gawmazar subareas.

It should be noted that geographic registration between various datasets is not always possible, because of differences in collection methods and resolution. The geographic accuracy and quality of each dataset is limited by the original source. Great efforts were made to ensure the accuracy of the HyMap data (Kokaly and others, 2008; Hoefen and others, 2010). However, exact registration between previously published known mineral occurrences, fault traces, geologic units, and structural boundaries in comparison to the HyMap data may not be ideal. To resolve additional details, the digital versions of these maps can be viewed at higher spatial resolution than what is possible in a single-page printed map.

A companion report and geodatabase of potential mineral resource anomalies (areas of a potential economic mineral resource occurrence) that have not been previously known or where the HyMap data have expanded the knowledge or surficial coverage can be found in King and others (2011b).

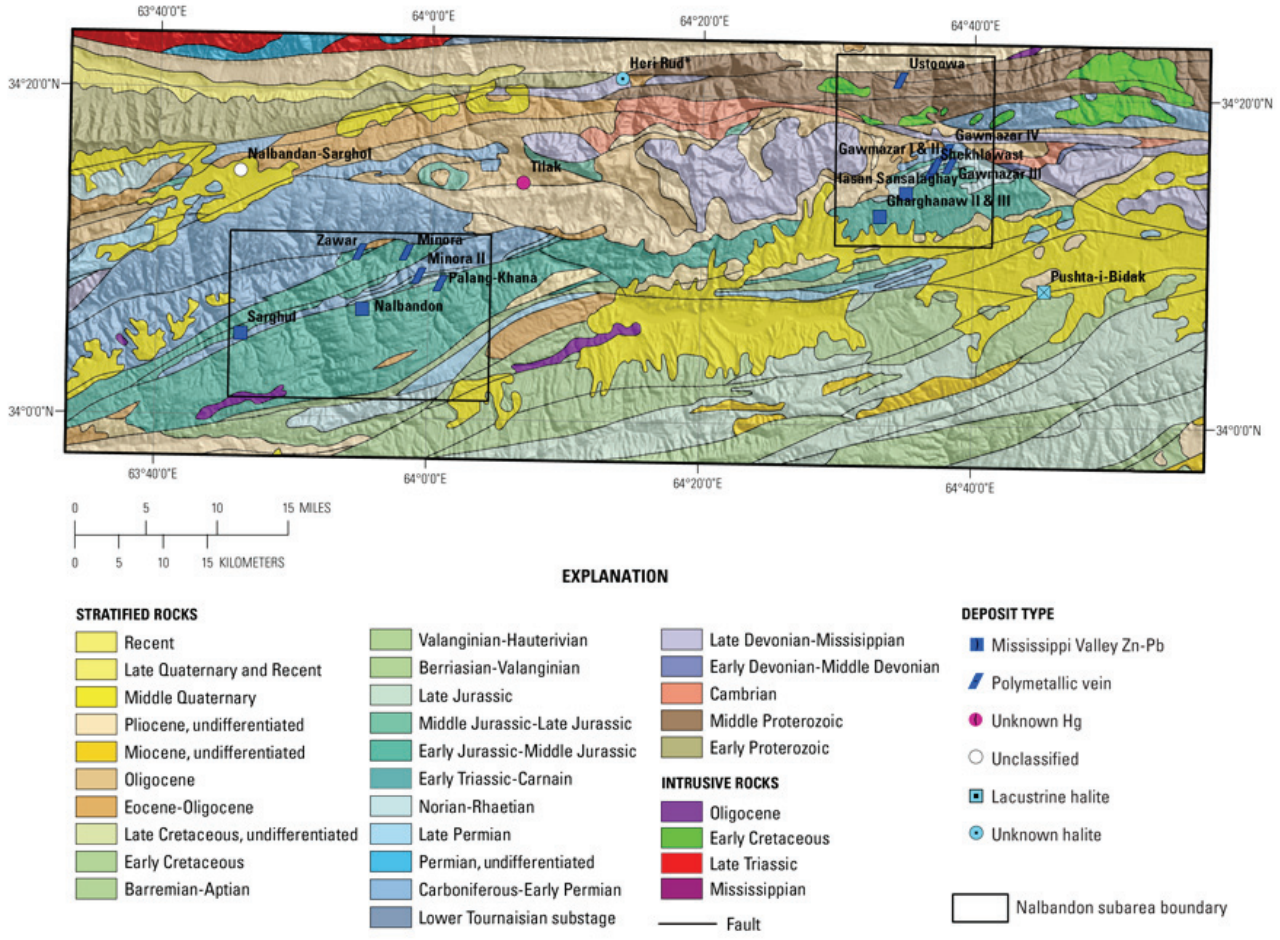

Figure 11B–5. Map showing location of known mineral occurrences in the Nalbandon area of interest (AOI). The map consists of four data layers: a shaded relief base map; a transparency of the geologic map (Doebrich and others,2006); fault traces (Peters and others, 2007); and known mineral occurrences (Peters and others, 2007). The map shows the overall AOI and two subareas: Nalbandon District and Gharghanaw-Gawmazar.

11B.3.1 Nalbandon Area of Interest

Figures 11B–6 and 11B–7 shows the distribution of carbonates, phyllosilicates, sulfates, altered minerals, other materials (32 possible classes), and the iron-bearing minerals (28 possible classes) for the entire Nalbandon AOI. HyMap data are also a powerful tool to use in the identification and mapping of faults and fractures (see fig. 11B–9); note the large Hari-Rud fracture system in the northern part of the image. The presence of clouds in an AOI is unusual because less than 5 percent of the total mapped area of Afghanistan is cloud covered in the HyMap dataset. Because of the large number of mineral classes represented and the subtleties of the distribution patterns in these maps, it is more instructive to display these results as a series of topical images depicting a group of minerals that are commonly related or occur together in special geologic environments (figs. 11B–8 to 11B–13). Figure 11B–8 shows the distribution of carbonate minerals in the AOI, whereas figure 11B–9 shows where the clays and micas were mapped. The distribution of iron oxide and hydroxide minerals are displayed in figure 11B–10. Secondary minerals are shown in figure 11B–11, and minerals commonly found in hydrothermally altered rocks are mapped in figure 11B–12.

11B.3.1.1 Carbonate Minerals

The calcite and calcite + muscovite/illite groups cover more than 90 percent of the mapped area and are continuous across most geologic boundaries. The widespread occurrence of carbonate minerals limits their usefulness for detecting areas characterized by calcite alteration (table 11B–1; fig. 11B–8). Although difficult to see because of the small number of pixels, dolomite and dolomite mixtures are present throughout the area, with small concentrations in the western and northeastern portion of the mapped area. The dolomite commonly occurs along or near fault/fracture boundaries.

11B.3.1.2 Clays and Micas

The phyllosilicates are the second most dominant group of minerals mapped in the AOI (fig. 11B–9). Muscovites and illites are the dominate minerals. Epidote and chlorite, when present, occur primarily in the western half of the area. The largest concentration of epidote and chlorite occurs in the Permian stratified rocks and intrusive units in the northernmost part of the AOI. Scattered and small clusters of epidote also occur in the Lower to Middle Jurassic, Permian, and Proterozoic geologic units. A small cluster of epidote pixels is present in the northeastern part of the area that cross-cuts geologic boundaries.

The kaolinite group of minerals primarily occur in the northern (Proterozoic and Carboniferous–Permian units) and southernmost portions of the area (see subarea maps for more detail). Although minor amounts of kaolinite group minerals occur in the Carboniferous–Lower Permian rocks in the west-central portion of the AOI.

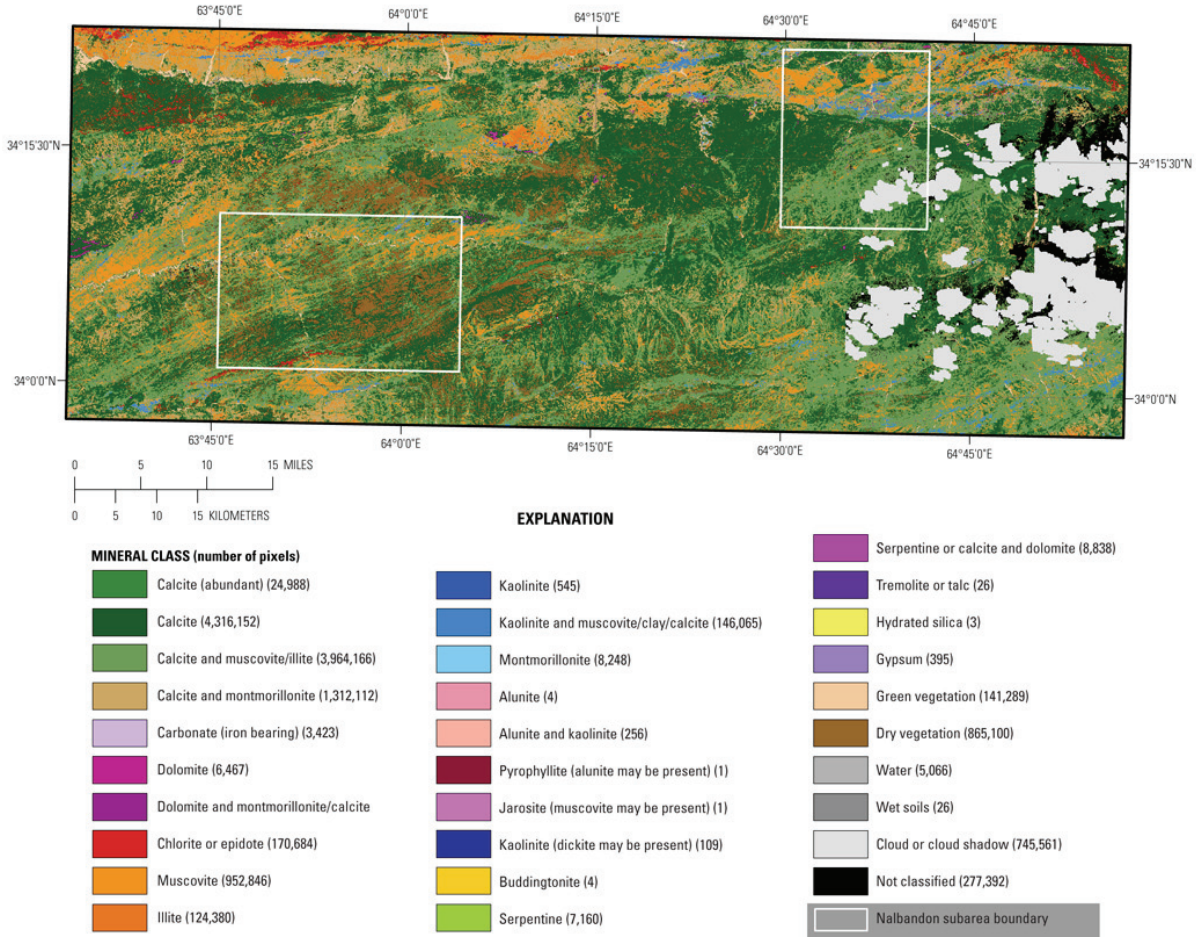

Figure 11B–6. Distribution of clays, carbonates, phyllosilicates, sulfates, altered minerals, and other materials detected in the HyMap data for the entire Nalbandon area of interest. The identification of the specific minerals is based on the presence of characteristic absorption features resulting from the vibrational process in the mineral. The map area was analyzed to detect the presence of 32 possible specific minerals or groups of minerals.

11B.3.1.3 Iron Oxides and Hydroxides

Figure 11B–10 shows the iron-bearing minerals in the Nalbandon AOI. These iron-bearing minerals can be roughly grouped into three zones that correlate with the geologic units (fig. 11B–4). The northern portion of the area, along and north of the Hari-Rud fracture zone, is dominated by Fe^{2+}- and Fe^{3+}-bearing minerals with minor amounts of hematite that occur along fractures and faults in the undifferentiated Pliocene rocks. The central portion of the map is dominated by the presence of dry vegetation and unclassified materials (see fig11B–6 for comparison) with lesser amounts of hematite (red), goethite (dark orange), and iron hydroxide minerals (light orange). Bedded units in the Lower–Middle Jurassic sedimentary rocks can be mapped, over tens of kilometers, by the presence of Fe^{3+} minerals (green). The southern (lower) portion of the map illustrates the lithologic control of the Fe^{2+}- and Fe^{3+}-bearing minerals in the Upper Jurassic to Lower Cretaceous rocks. Hematite minerals (red) occur along and between narrowly separated fractures and faults. Mineral occurrence and distribution may be masked in the central part of the AOI because of the presence of vegetation.

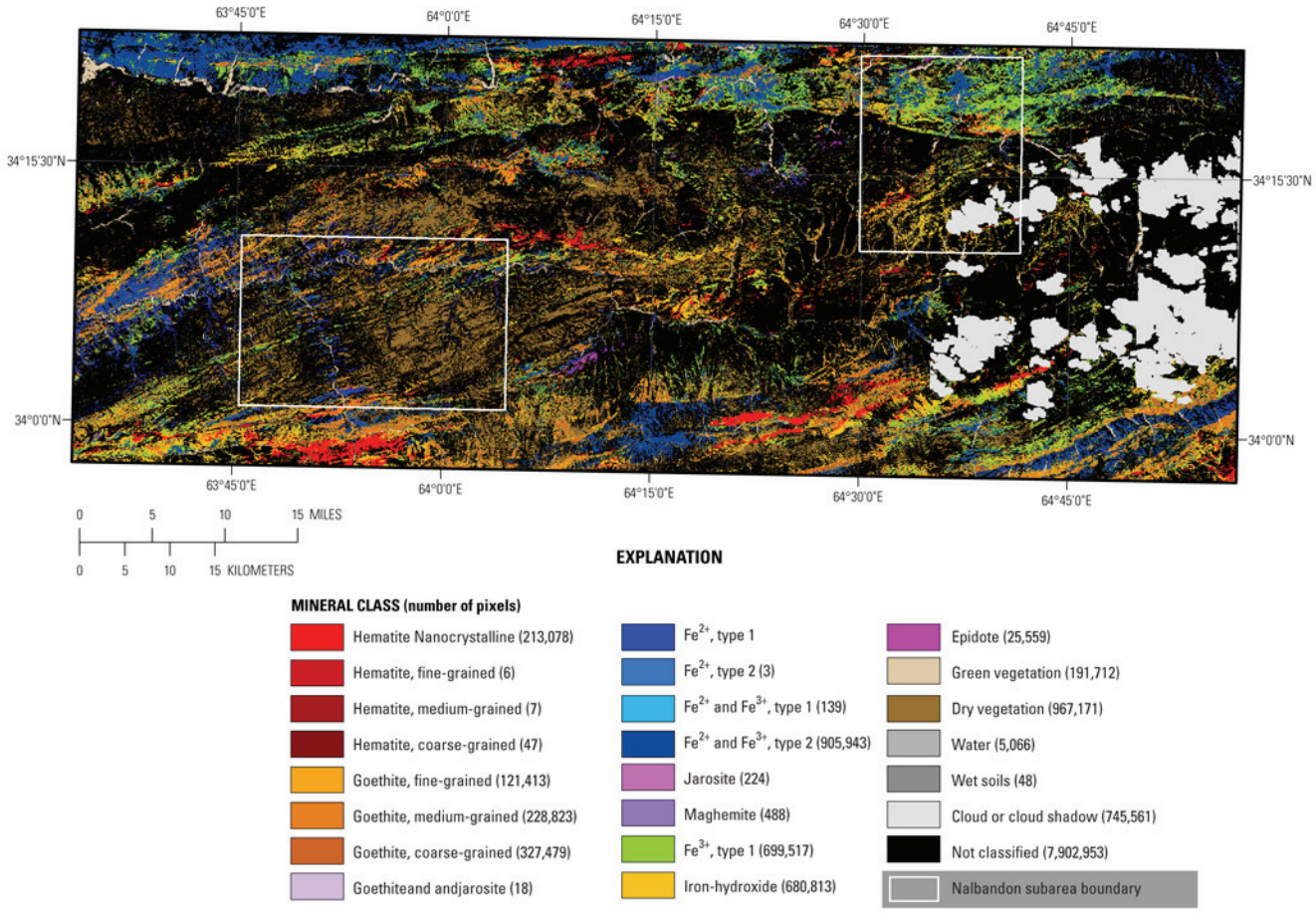

Figure 11B–7. Image showing iron-bearing minerals and other materials in the Nalbandon area of interest that were detected in the HyMap data.

11B.3.1.4 Common Secondary Minerals

The occurrence and distribution of common secondary minerals for the AOI are shown in figure 11B–11. This map shows information taken from both the 1- and 2-µm-wavelength datasets. A coherent grouping of secondary minerals occurs adjacent and north of the Hari-Rud fracture zone. In the central part of the AOI (adjacent to the Nalbandon District subarea), a small concentration of serpentine and serpentine or calcite + dolomite was mapped. Common secondary minerals in the southern half of the AOI fail to show a coherent distribution.

11B.3.1.5 Common Alteration Minerals

Most of the minerals in this group are commonly present in hydrothermally altered rocks associated with epithermal processes. Consequently, where they occur in distinct clusters is of great interest in terms of potential mineral deposits. However, only a single pixel or small number of pixels of the individual minerals were mapped in the area (fig. 11B–12). Occurrence of two or more minerals associated with hydrothermal alteration processes are observed in the Proterozoic rocks in the northernmost portion of the AOI. In the northern part of the AOI, epidote or chlorite are shown to be spatially related to the occurrence of the kaolinite group of minerals.

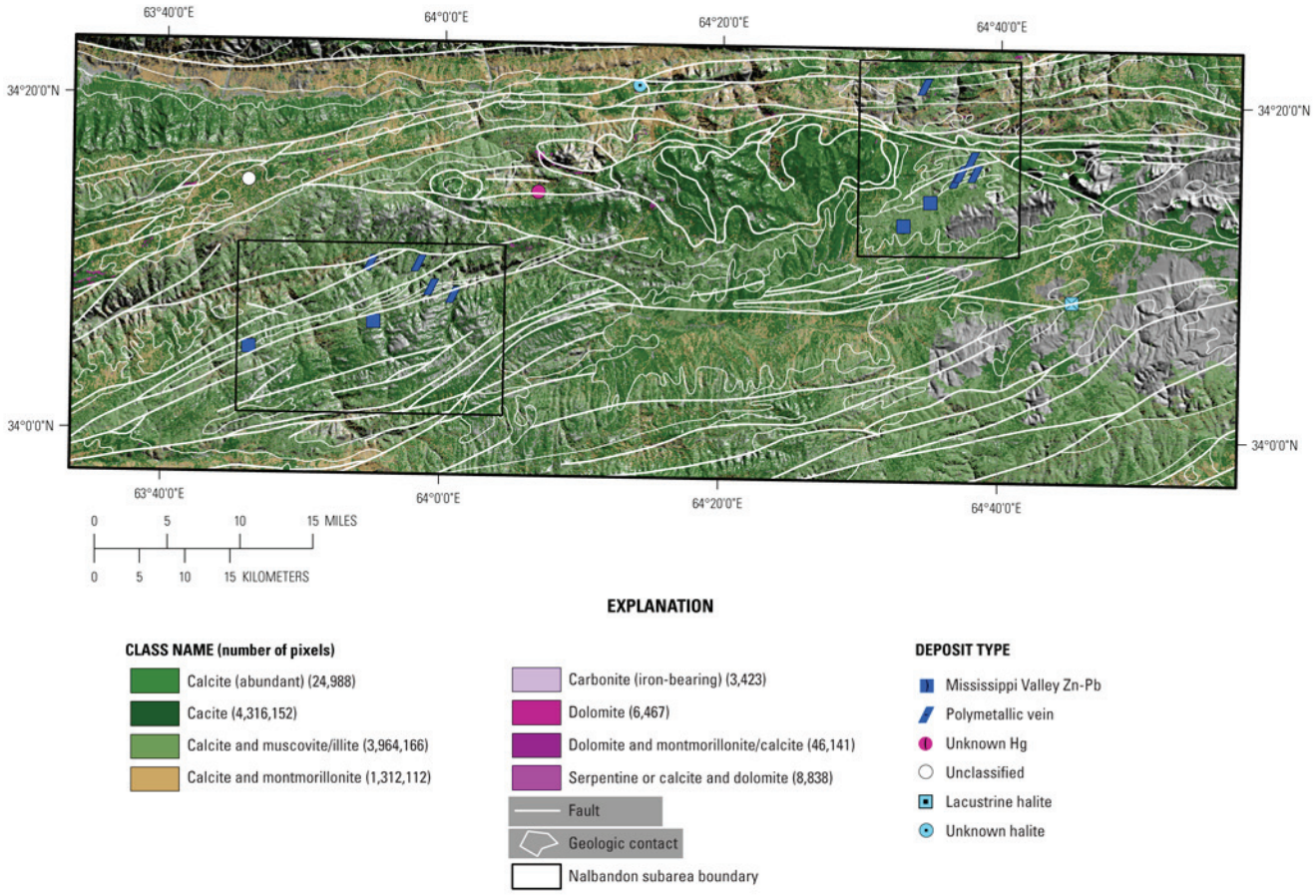

Figure 11B–8. Distribution of carbonate-bearing minerals detected by the HyMap data in the Nalbandon area of interest.

11B.3.2 Gharghanaw Gawmazar Subarea:

The known mineral occurrence map (semitransparent geologic map overlain on a shaded relief image) shows the position of reported mineral occurrences in the Gharghanaw Gawmazar area (fig. 11B–13). The topography in the area ranges from 2,020 to 3,308 m and no rivers are present in the area (fig. 11B–14).

The geologic map of the area (fig. 11B–15) shows rocks ranging in age from Mesoproterozoic to middle Quaternary age. Early Cretaceous intrusive rocks occur in the northern part of the area along the Hari Rud fault. The majority (7 of 10) of the known mineral occurrence in Gharghanaw-Gawmazar occur south of the Hari Rud fault zone in rocks of Early–Middle Jurassic age.

The Upper Triassic (Norian–Rhaetian) and Oligocene geologic units in the central part of the area are easily recognized by their bluish-purple shades in the Landsat Enhanced Thematic Mapper (TM) data (Davis, 2007) (fig.11B–15). The Hari Rud fracture zone is readily identified in the central part of the image.

Figures 11B–17 and 11B–18 show the distribution of iron-bearing and carbonate, sulphate, phyllosilicate, and altered minerals, respectively. The map of iron-bearing minerals (fig. 11B–17) also shows a variation in the mineral assemblages on either side of the large fault zone. Fe^{2+} and Fe^{3+} minerals are pervasive in the Proterozoic rocks. South of the Hari-Rud fault zone, the surficial mineralogy is dominated by iron hydroxides and goethites.

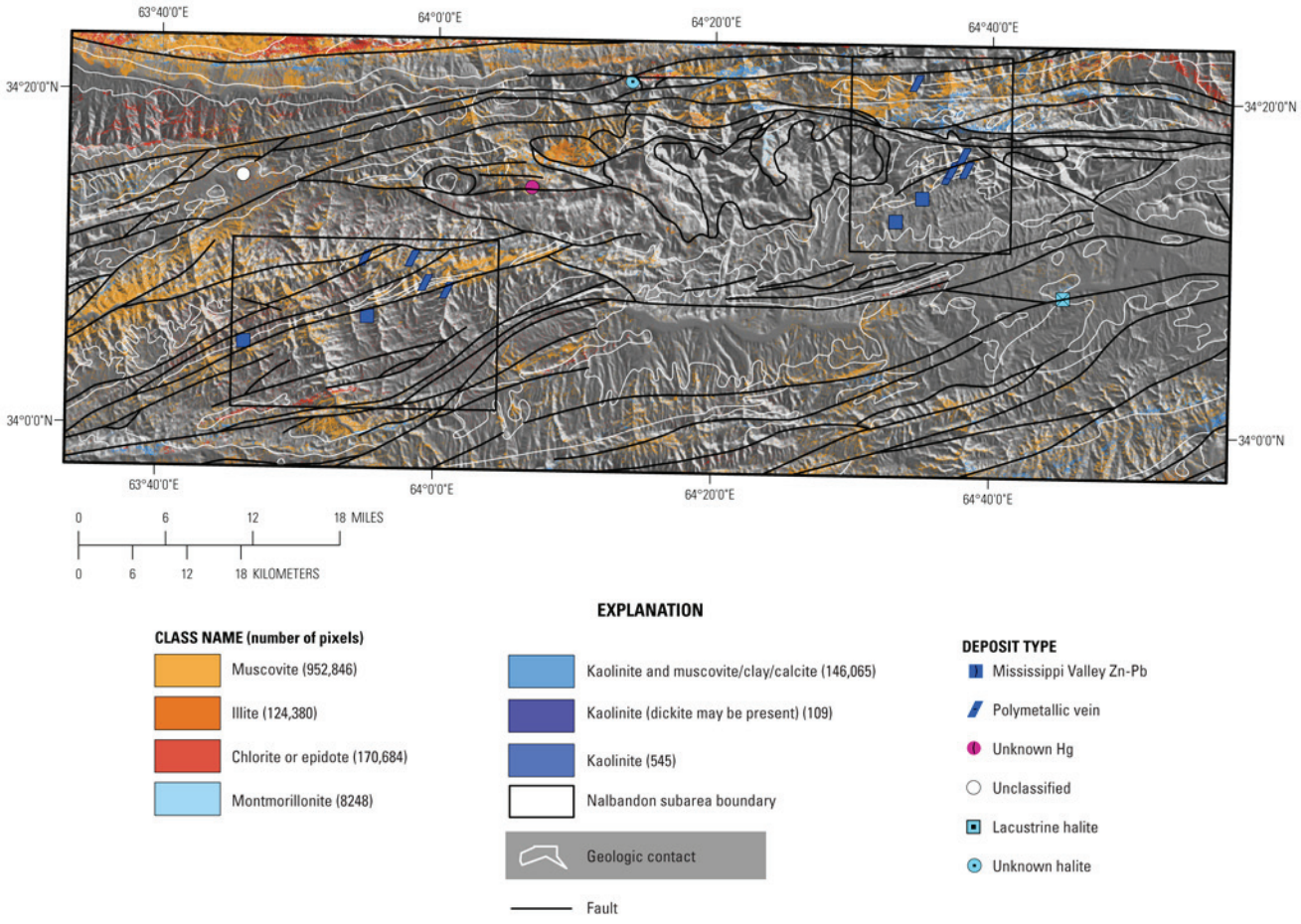

Figure 11B–9. Distribution of clays and micas identified in the HyMap data for the Nalbandon area of interest.

11B.3.2.1 Gharghanaw-Gawmazar Subarea: Carbonate Minerals

Calcite-rich rocks are widespread and occur over the entire subarea (fig.11B–19). A lesser number of pixels representing dolomite and dolomite mixtures are present throughout the area with small concentrations in the western and northeastern portion of the mapped area. The dolomite occurs in Devonian rocks in the western part of the area and along or near fault traces or edges of intrusive bodies in the northeast part of the image.

11B.3.2.2 Gharghanaw-Gawmazar Subarea: Clays and Micas

On the basis of the HyMap data, figure 11B–20 shows the enrichment of clays and micas in the Proterozoic rocks and Norian–Rhaetian age rocks in the Gharghanaw-Gawmazar subarea. The clays and micas are associated with the Mesoproterozoic rocks north of the Hari Rud fault zone. The muscovites are present in the Proterozoic rocks. Polymetallic veins and lead-zinc deposits are known to occur along the boundary of the Norian–Rhaetian and Early–Middle Jurassic age rocks (fig. 11B–13) and show no correlation with the phyllosilicate minerals.

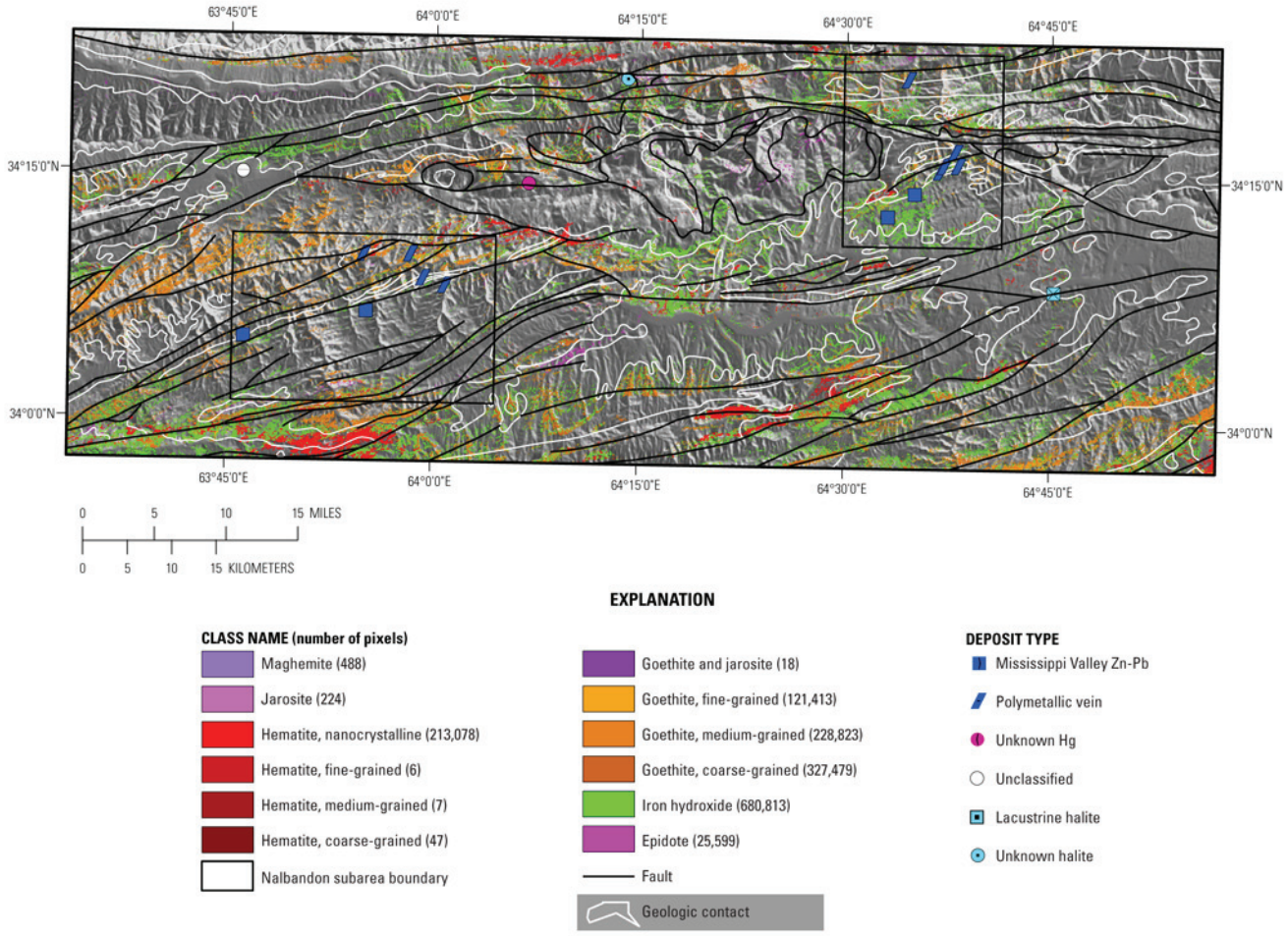

Figure 11B–10. Distribution of iron hydroxides and oxides mapped using the HyMap data for the Nalbandon area of interest.

11B.3.2.3 Gharghanaw–Gawmazar Subarea: Iron Oxide and Hydroxide Minerals

Figure 11B–21 shows the distribution of iron oxides and hydroxides in the Gharghanaw-Gawmazar subarea. Hematite is primarily mapped adjacent to contact zones of the Early Cretaceous intrusive rocks and the Proterozoic country rocks. However, a cluster of hematite is also present in the southern part of the area at the terminus of a fault zone (King and others, 2011a). Mineral occurrence and distribution may be somewhat masked in the central portion of the area because of the presence of dry vegetation.

11B.3.2.4 Gharghanaw-Gawmazar Subarea: Common Secondary Minerals

There are few occurrences and scattered distribution of common secondary minerals (fig.11B–22) in the area. The largest number of pixels of secondary minerals occurs in the Pliocene rocks in the northernmost part of the area.

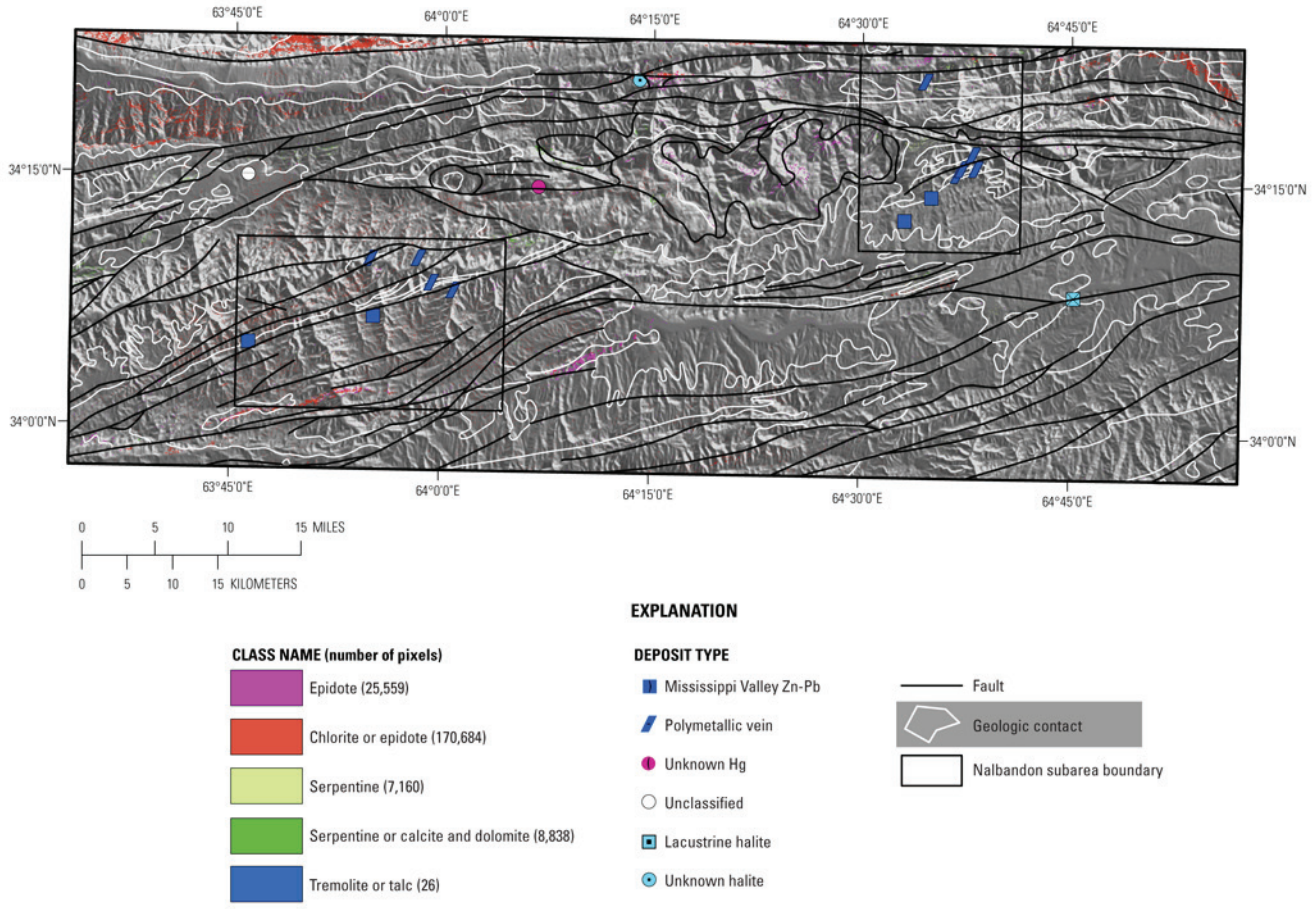

Figure 11B–11. Occurrence and distribution of common secondary minerals detected in the HyMap data.

11B.3.2.5 Gharghanaw-Gawmazar Subarea: Common Alteration Minerals

Common alteration materials detected in the HyMap data (fig. 11B–23) in the area are primarily kaolinite group minerals that are present in the Mesoproterozoic rocks. The few pixels of chlorite or epidote minerals are present in Pliocene rock in the northernmost part of the image (fig. 11B–23).

11B.3.3 Nalbandon District Subarea

The known mineral occurrence map (fig. 11B–24) shows the position of reported mineral occurrences in the Nalbandon District subarea. The topography in the area ranges from 1,435 to 3,488 m and two rivers, one flowing east-west and one north-south, are present in the area (fig. 11B–25). Figure 11B–26 shows that the district is composed of dominantly Early–Middle Jurassic age rocks with some of Carboniferous–Early Permian age units.

In the Landsat TM data (Davis, 2007), the Early–Middle Jurassic age rocks in the central part of the area are easily recognized by their distinct bedding and bluish-brown color (fig.11B–27). The majority (5 of 6) of the known mineral occurrence in the Nalbandon District occur in rocks of Early–Middle Jurassic age (fig. 11B–24).

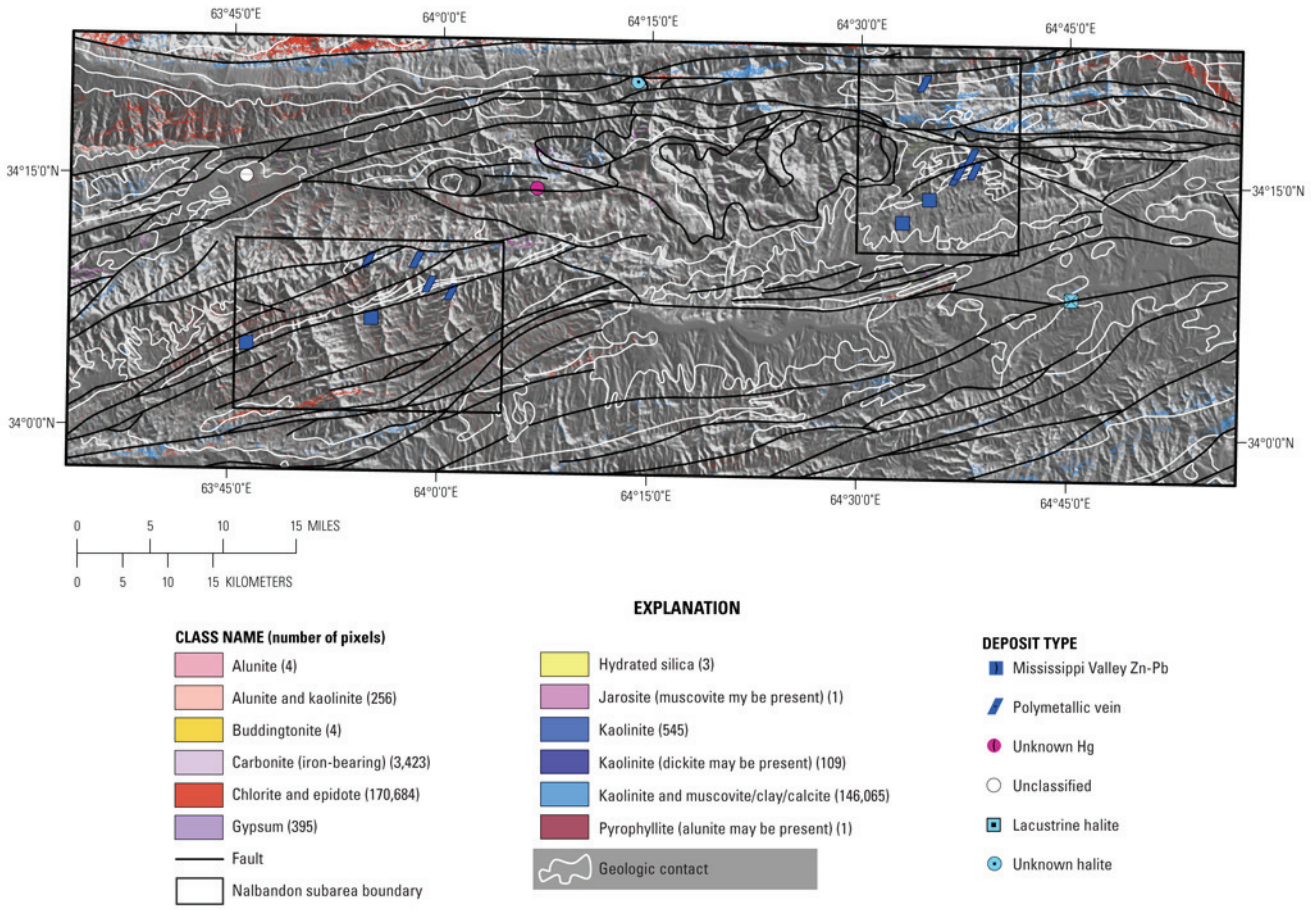

Figure 11B–12. Distribution of common alteration minerals in Nalbandon area of interest.

The overall-inclusive imaging spectrometer data for the area (figs. 11B–28 and 11B–29) show the distribution of iron-bearing minerals and carbonate, phyllosilicate, sulphate, alteration minerals, and other materials respectively. Dry vegetation (brown) is abundant throughout the entire subarea, but is most pervasive in the eastern half. The presence of the dry vegetation (figs. 11B–28 and 11B–29) masks much of the area and reduces the mineral identification in areas with significant vegetation cover.

11B.3.3.1 Nalbandon District Subarea: Carbonate Minerals

Figure 11B–30 shows widespread distribution of carbonate-rich rocks over the entire AOI. Calcite and calcite and muscovite or illite are by far the dominant mineral groups.

11B.3.3.2 Nalbandon District Subarea: Clays and Micas

Figure 11B–31 shows the enrichment of phyllosilicates in the Nalbandon District subarea. Muscovite (lighter orange) occurs throughout the area. Although chlorite or epidote is mapped throughout the area in scattered pixels, a large concentration of pixels is located adjacent and east of the Oligocene intrusive outcrop in rocks mapped as Early–Middle Jurassic age (fig. 11B–26). These chlorite or epidote rocks are not reported as common occurrences in the Jurassic age rocks and warrant additional consideration (King and others, 2011a). An anomalous occurrence of kaolinite group minerals occurs in the northernmost part of the district.

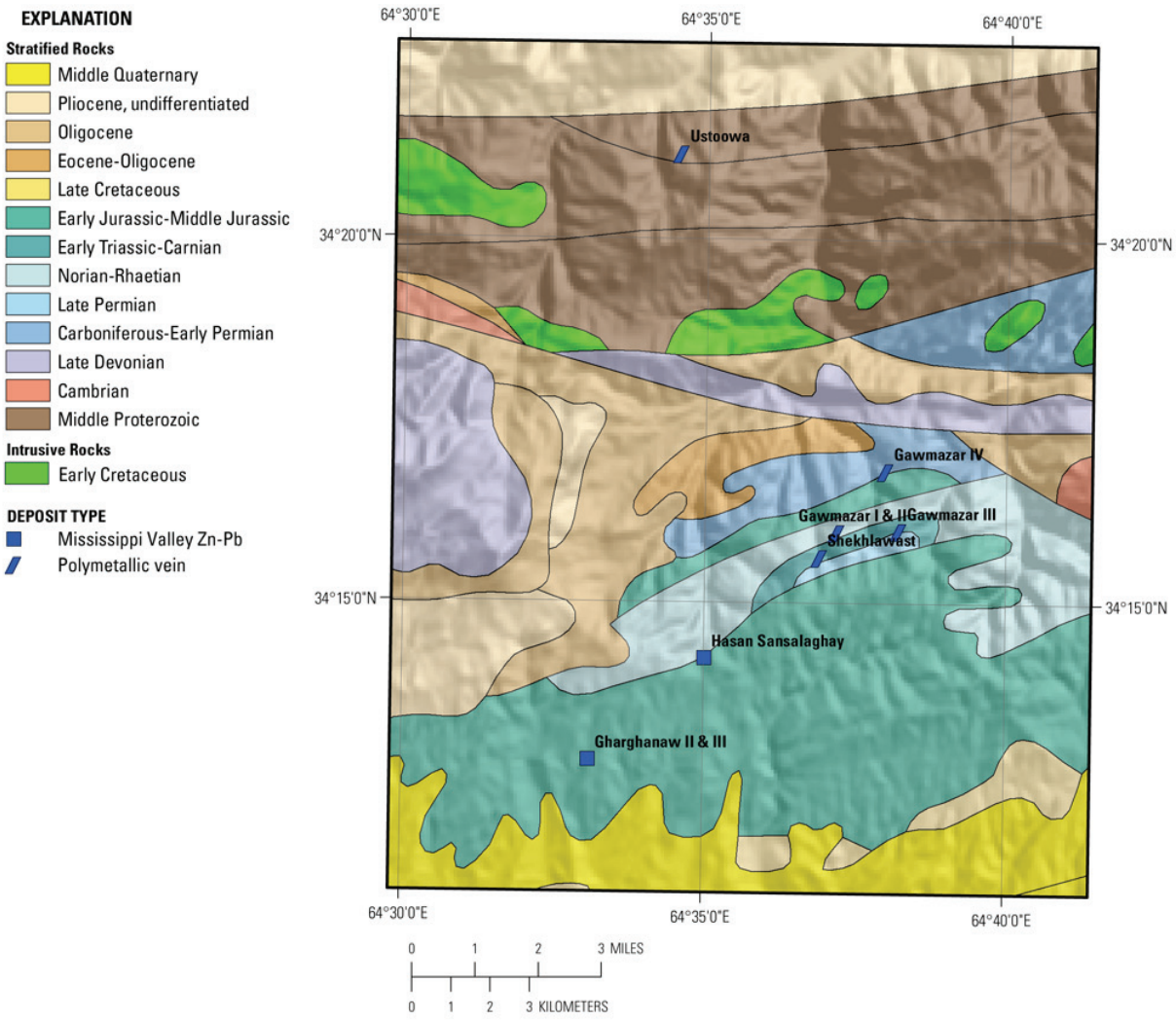

Figure 11B–13. Known mineral occurrences in the Gharghanaw-Gawmazar subarea of the Nalbandon area of interest.

11B.3.3.3 Nalbandon District Subarea: Iron Oxides and Hydroxides

The distribution of iron oxides and hydroxides is shown figure 11B–32. Hematite is primarily present adjacent to contact zones of Early Cretaceous intrusive rocks and Proterozoic country rocks. However, a cluster of hematite is also present in the southern part of the area at the terminus of a fault zone (King and others, 2011a). Mineral occurrence and distribution may be somewhat masked in the central portion of the AOI because of the presence of dry vegetation.

11B.3.3.4 Nalbandon District Subarea: Common Secondary Minerals

There are few occurrences of common secondary minerals (fig.11B–33), with the exception of the chlorite or epidote group, which seems to be present throughout the subarea with concentrated areas along the south-central portion of the AOI. A coherent grouping of secondary minerals occurs in the northern part of the AOI. These occurrences are related to geologic units adjacent and north of the Hari-Rud fracture zone. Small concentrations of serpentine and serpentine or calcite and dolomite were

mapped in the central portion of the area, and the southern half of the AOI shows only scattered occurrences.

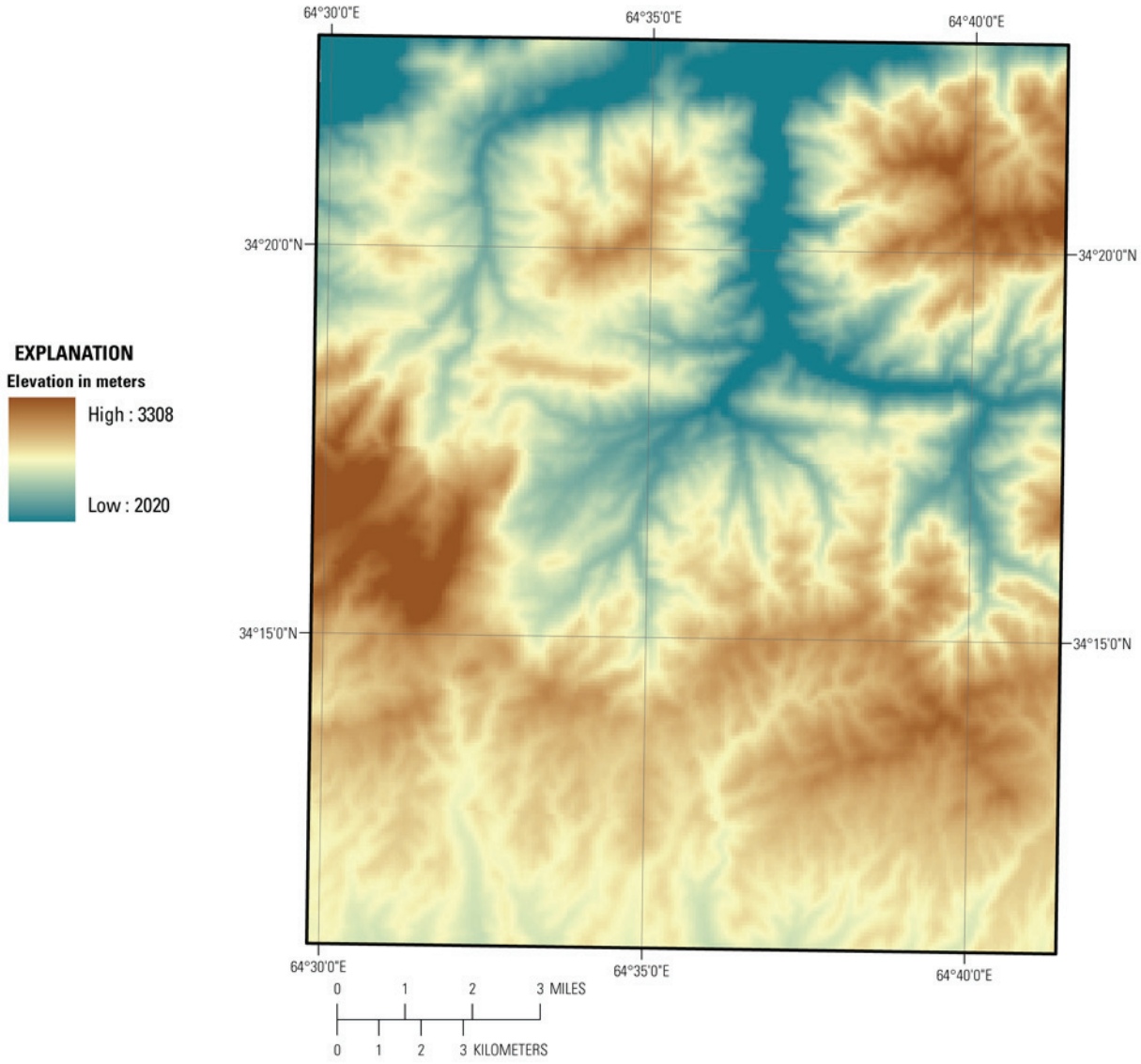

Figure 11B–14. Shaded relief map showing that elevation in the Gharghanaw-Gawmazar subarea of the Nalbandon area of interest ranges from 2,020–3,308 meters. The darker brown tones indicate the higher elevations and the lower elevations are represented by the blue tones.

11B.3.3.5 Nalbandon District Subarea: Common Alteration Minerals

The only significant common alteration minerals that do not have a seemingly random distribution are the kaolinite group minerals, which map along the northeastern portion of the AOI and the previously mentioned chlorite or epidote group (fig. 11B–34). In addition, a cluster of alunites and kaolinites is seen north of the Minora mineral occurrence and is discussed in the USGS anomaly report (King and others, 2011a).

11B.4 Summary

The horizontally bedded geologic units (little horizontal surface expression in areas with steep terrain), the alteration mineral assemblages and patterns associated with lead-zinc deposits, and the presence of abundant dry vegetation that may have masked the surficial minerals in a significant and geologically important part of the area have reduced the utility of the imaging spectrometer data for overall site characterization in the Nalbandon AOI.

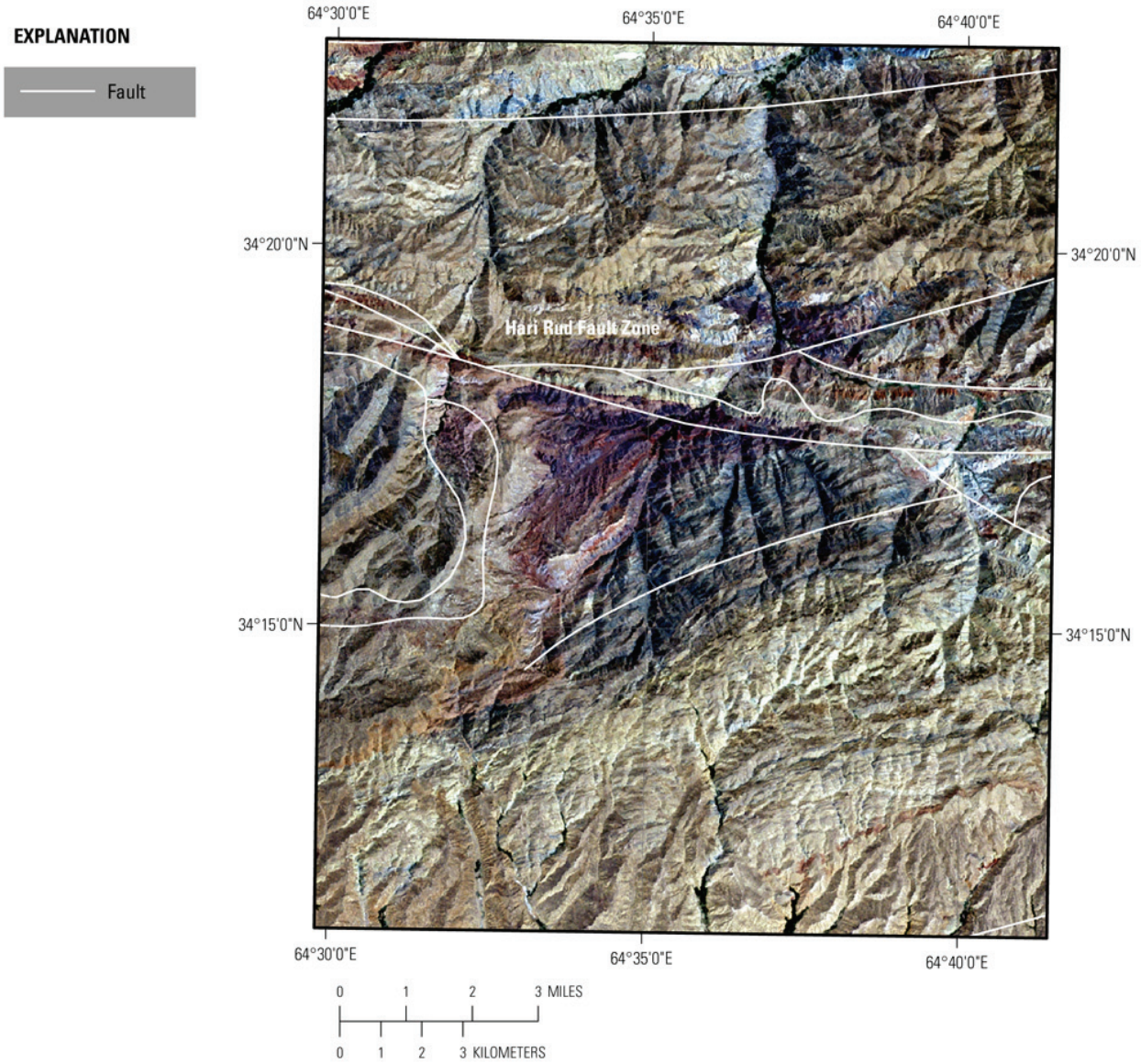

Figure 11B–15. Numerous faults and fractures of different orientations and extent occur in the Gharghanaw-Gawmazar subarea of the Nalbandon area of interest. The fault traces (Peters and others, 2007) are placed on Landsat TM images (Davis, 2007). Marked color differences in the TM data are associated with rocks of different ages.

The imaging spectrometer data for the Nalbandon District subarea suggest that the known mineral occurrence at Palang-Khana, Nalbandon, and Sarghul are in mappable lithologic units consisting of a mixture of Fe^{3+} minerals, iron hydroxide, and goethite. It is believed that additional field verification would confirm this observation as this type of mineral assemblage extends across the area.

The HyMap data show that the Gawmazar polymetallic-vein mineral occurrences and the Gharghanaw II and III lead-zinc mineral occurrences (fig. 11B–13) are preferentially in units that were mapped as enriched concentrations of iron hydroxide, although there was not a high correlation.

Attempts to verify areas of hydrothermal alteration identified in field studies by the Lithuanians (Motza and Silaupa, 2010) using the HyMap data did prove effective. There were no indications of minerals associated with hydrothermal alteration (fig. 11B–12) in the HyMap data. Again, this may be due to the size of the reported field observations or the location of the alteration in the geologic sequence. If the alteration is bedded in steep-sided exposures with little horizontal exposure, the HyMap data may not have detected the occurrence.

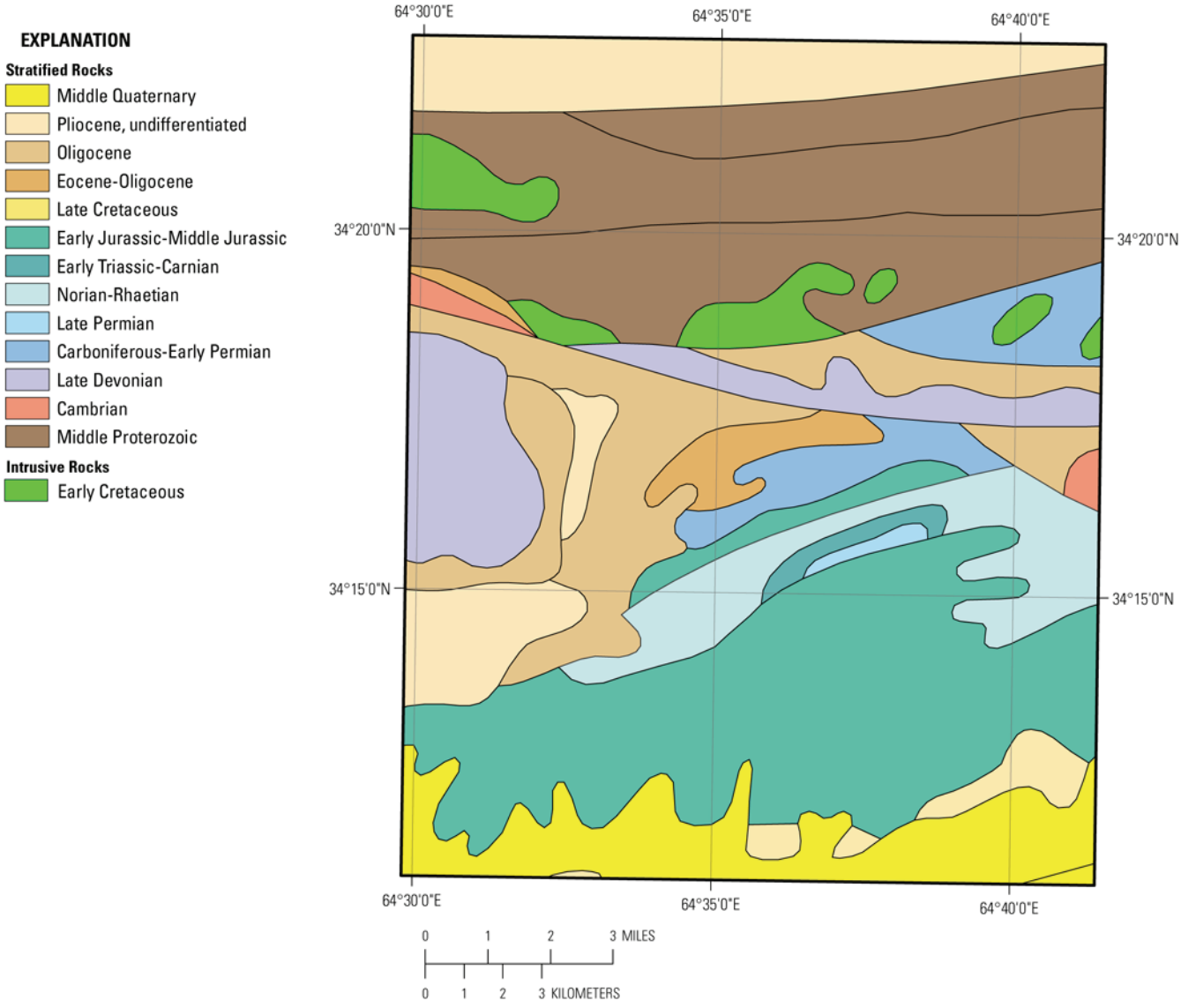

Figure 11B–16. Geologic map of the Gharghanaw-Gawmazar subarea of the Nalbandon area of interest from Doebrich and others (2006).

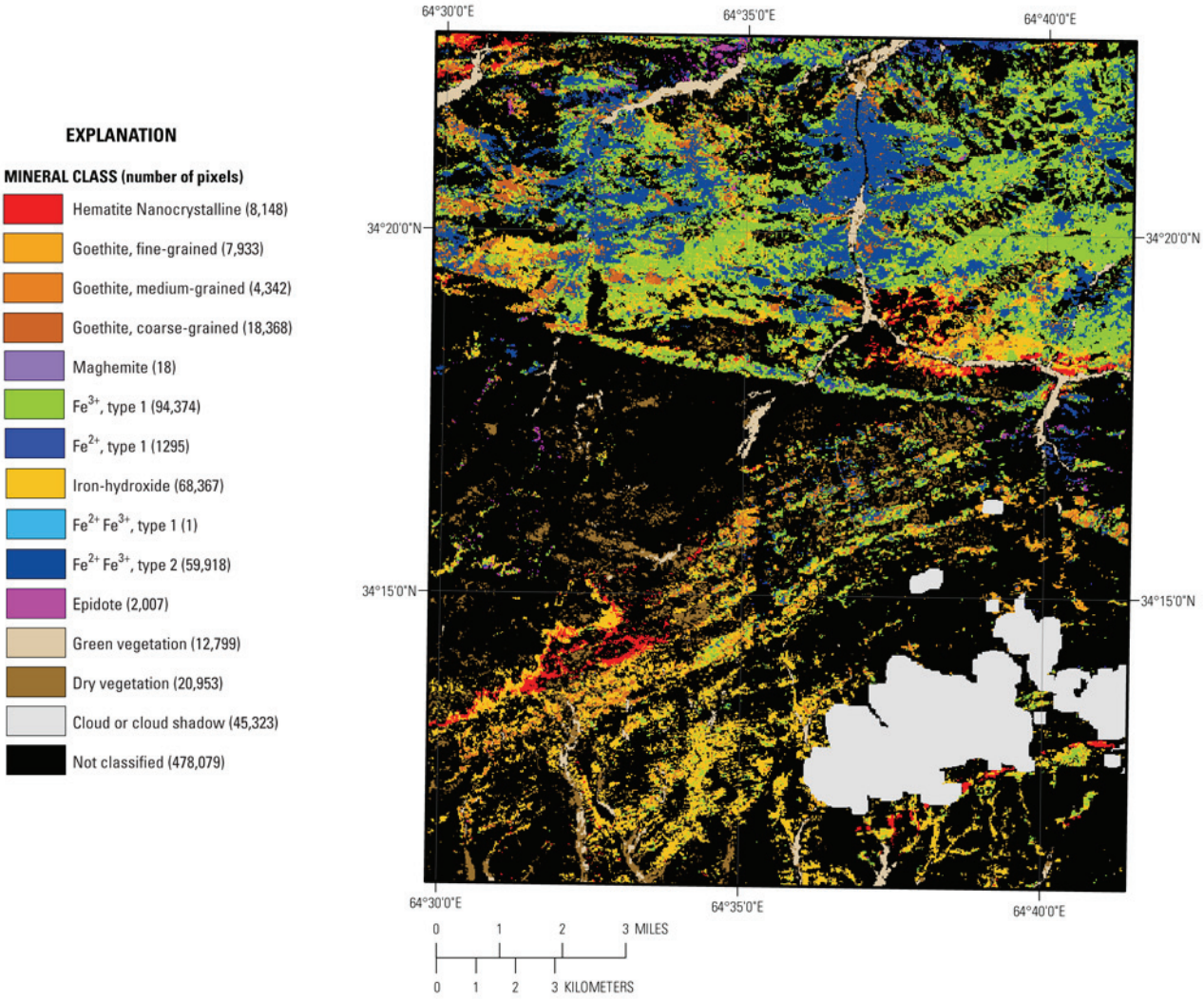

Figure 11B–17. The iron-bearing and other alteration minerals detected in the HyMap data for the Gharghanaw-Gawmazar subarea of the Nalbandon area of interest are shown in this image.

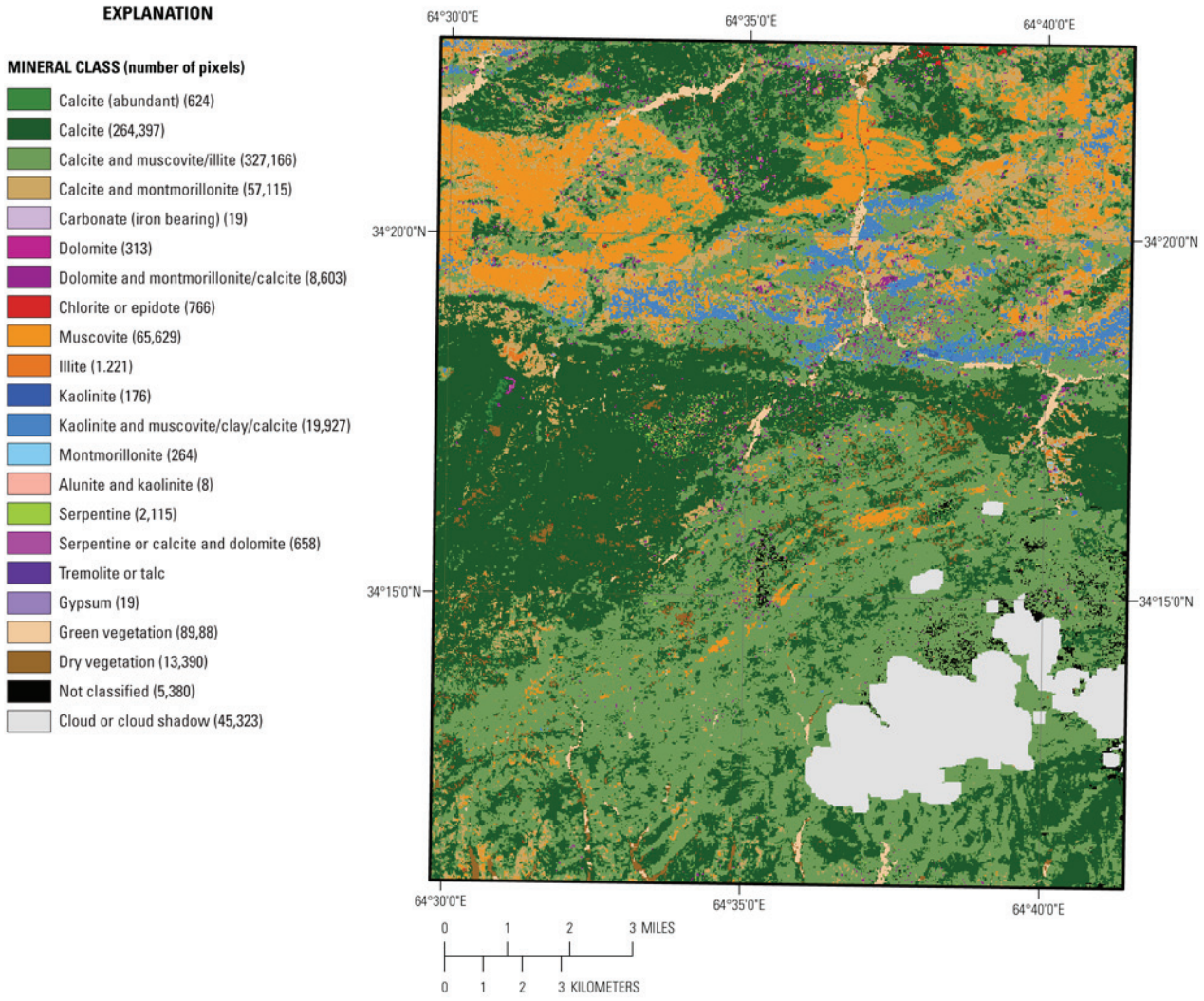

Figure 11B–18. Distribution of clays, carbonates, phyllosilicates, sulfates, altered minerals, and other materials for the Gharghanaw-Gawmazar subarea of the Nalbandon area of interest based on the HyMap data.

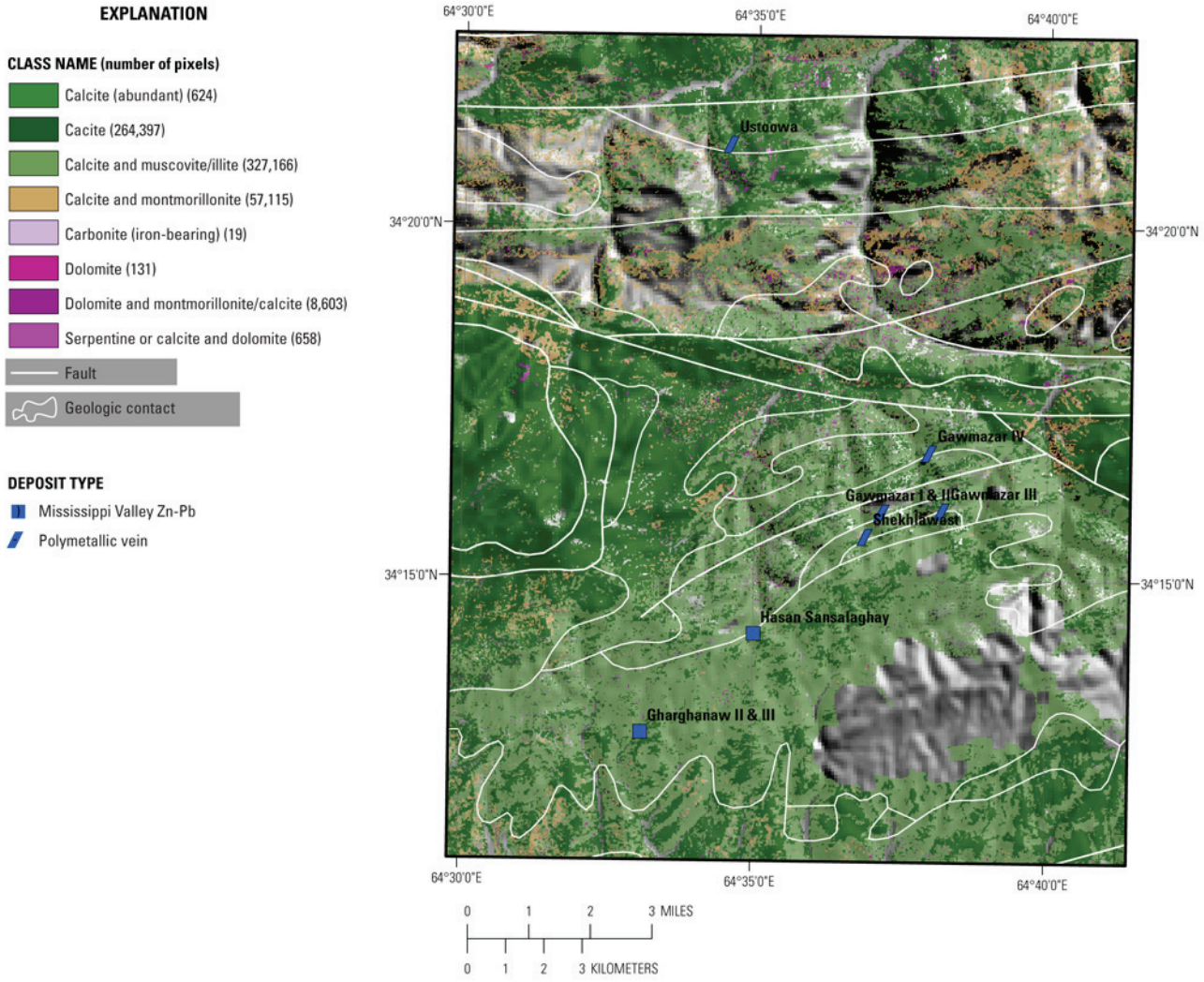

Figure 11B–19. Distribution of carbonate-bearing minerals in the Gharghanaw-Gawmazar subarea detected in the HyMap data.

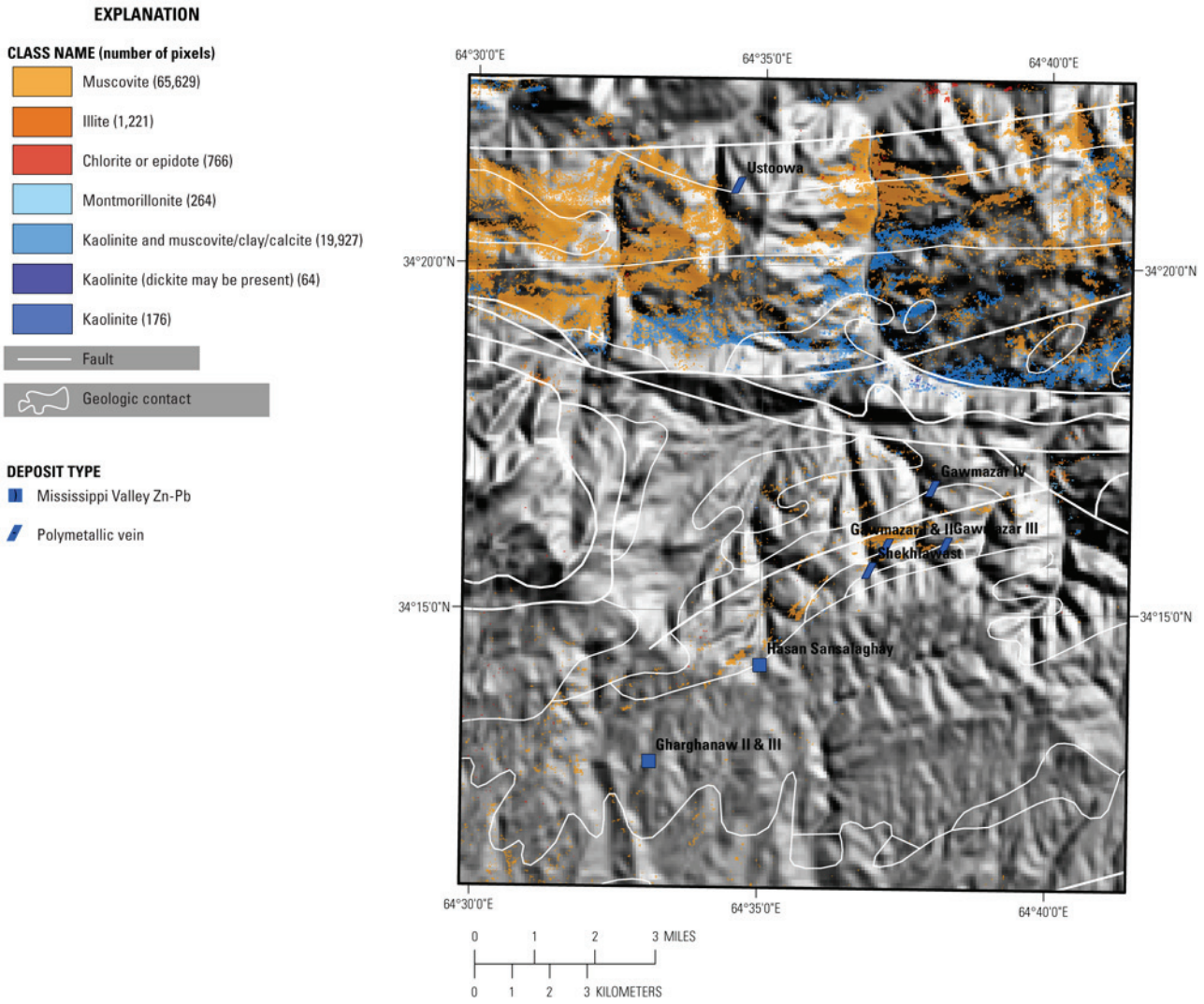

Figure 11B–20. Distribution of clays and micas detected using the HyMap data. The figure shows the occurrence of muscovites and illites and epidote and kaolinite group of minerals.

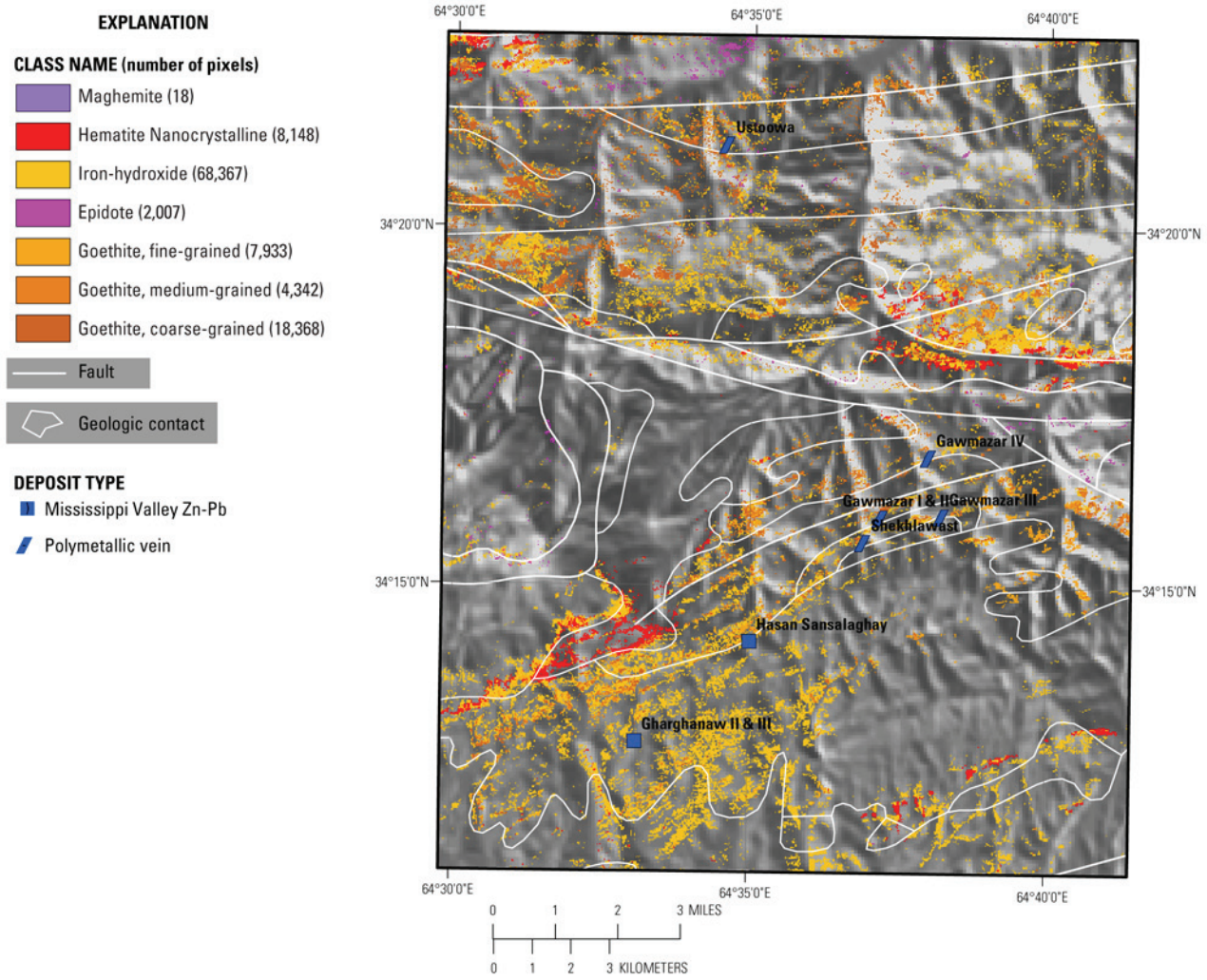

Figure 11B–21. Distribution of Fe-hydroxides and oxides for the Gharghanaw-Gawmazar subarea.

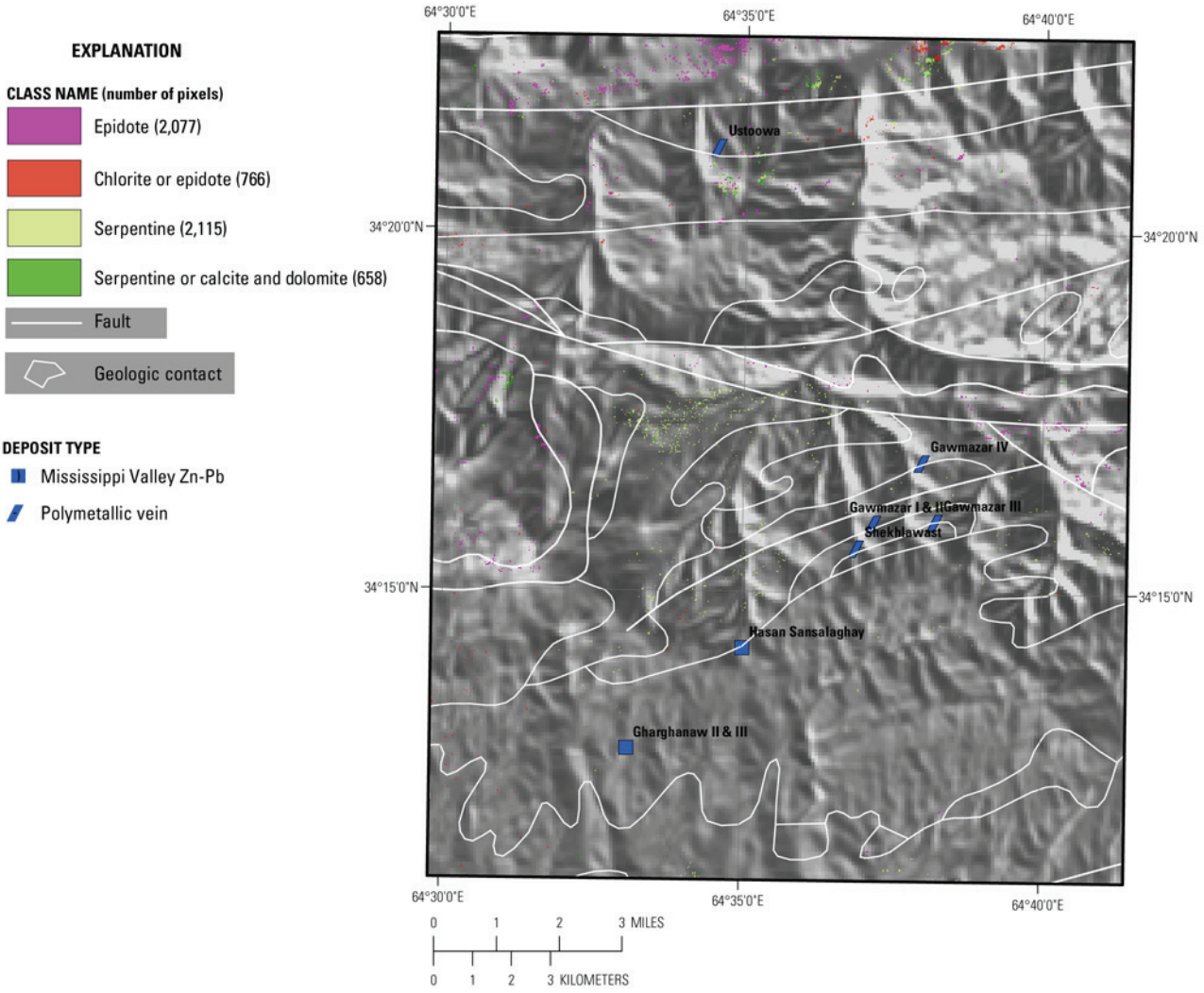

Figure 11B–22. This image shows the very limited occurrence and scattered distribution of common secondary minerals detected in the HyMap data. A coherent grouping of secondary minerals occurs in the northern part of the Nalbandon area of interest.

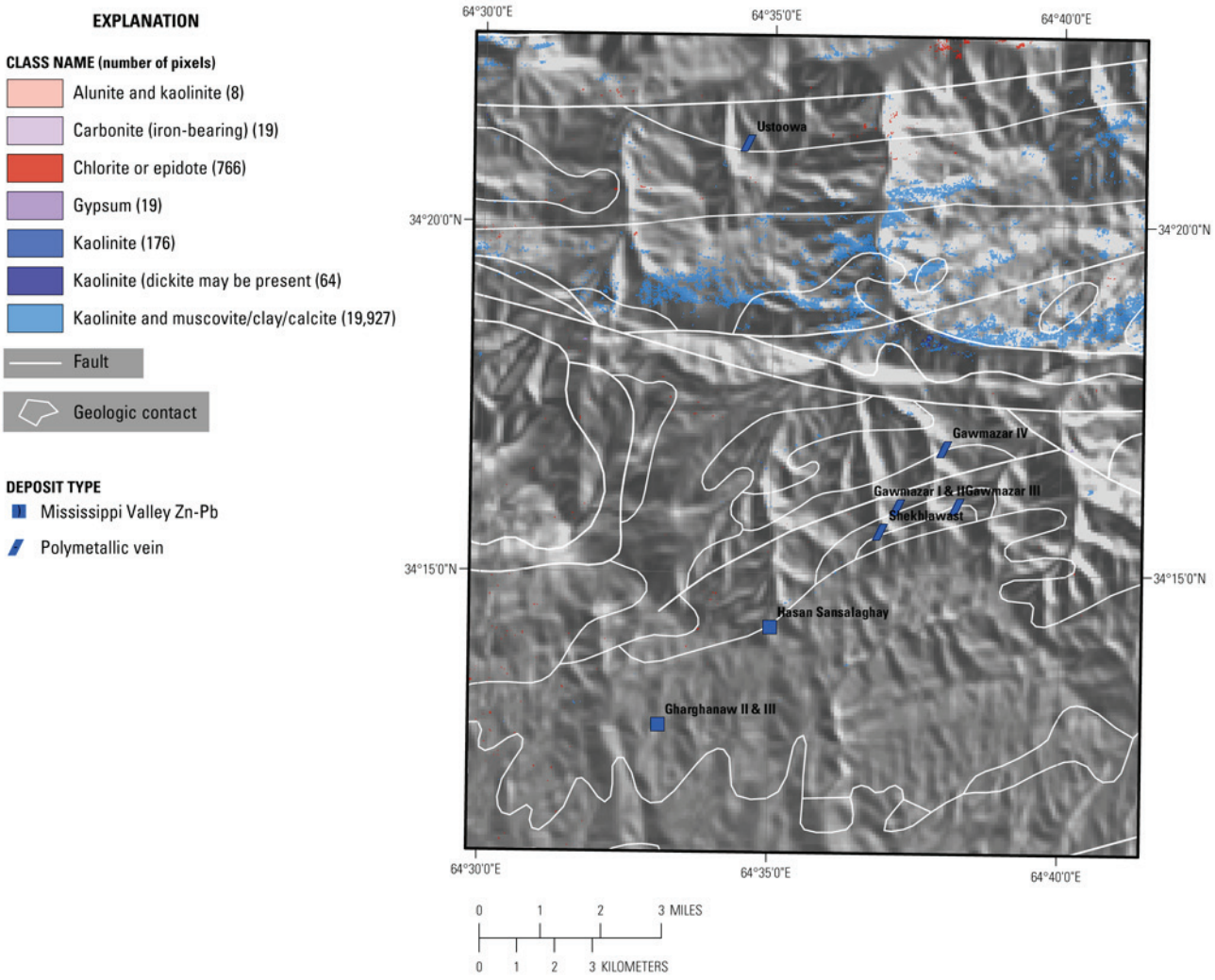

Figure 11B–23. Common alteration materials detected in the HyMap data are limited primarily to kaolinite group minerals.

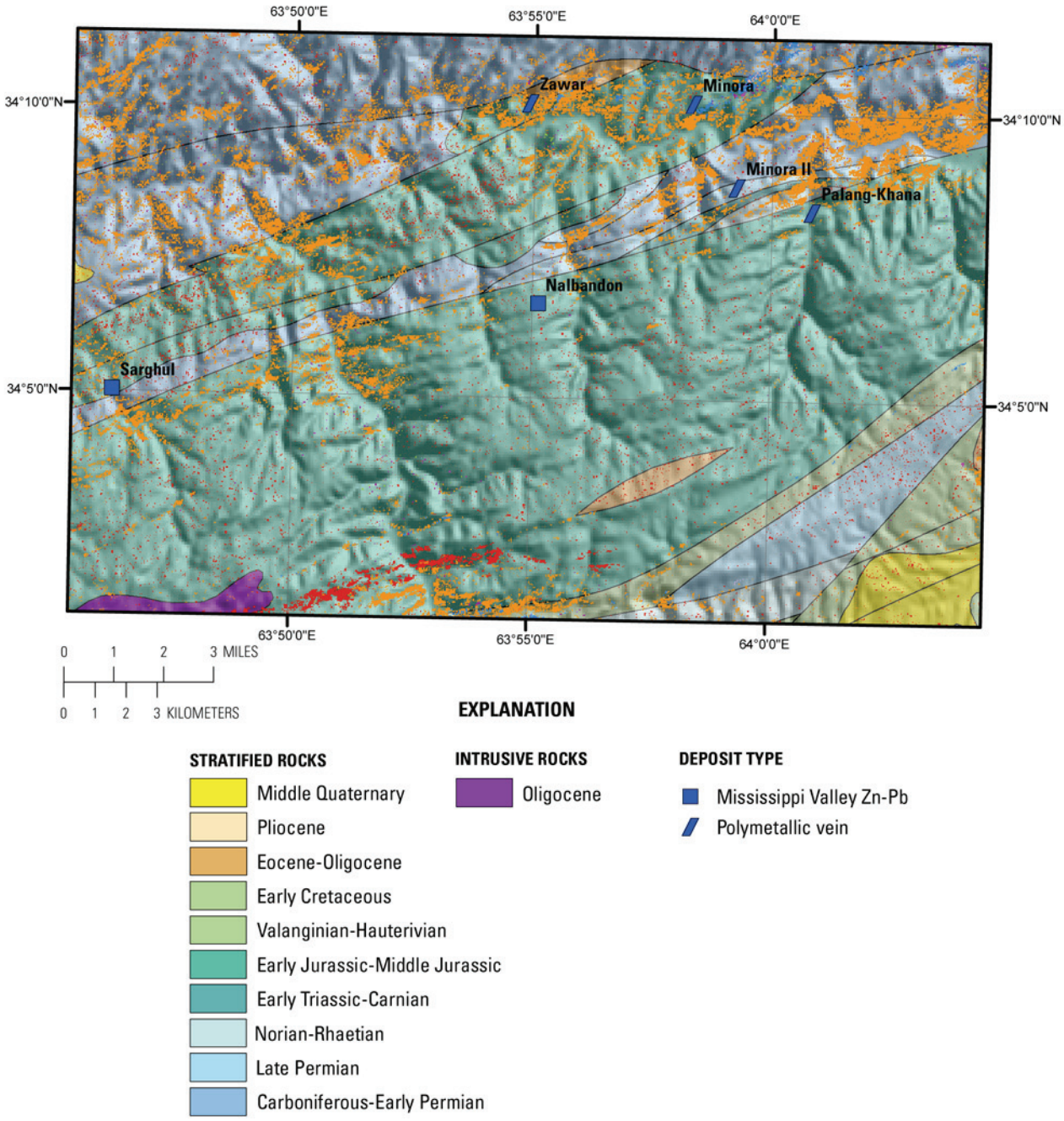

Figure 11B–24. This map shows the known mineral occurrences in the Nalbandon District subarea of the Nalbandon area of interest. The district includes four polymetallic-vein occurrences (Palang-Khana, Zawar, Minora, and Minora II) and two lead-zinc occurrences (Nalbandon and Sarghul).

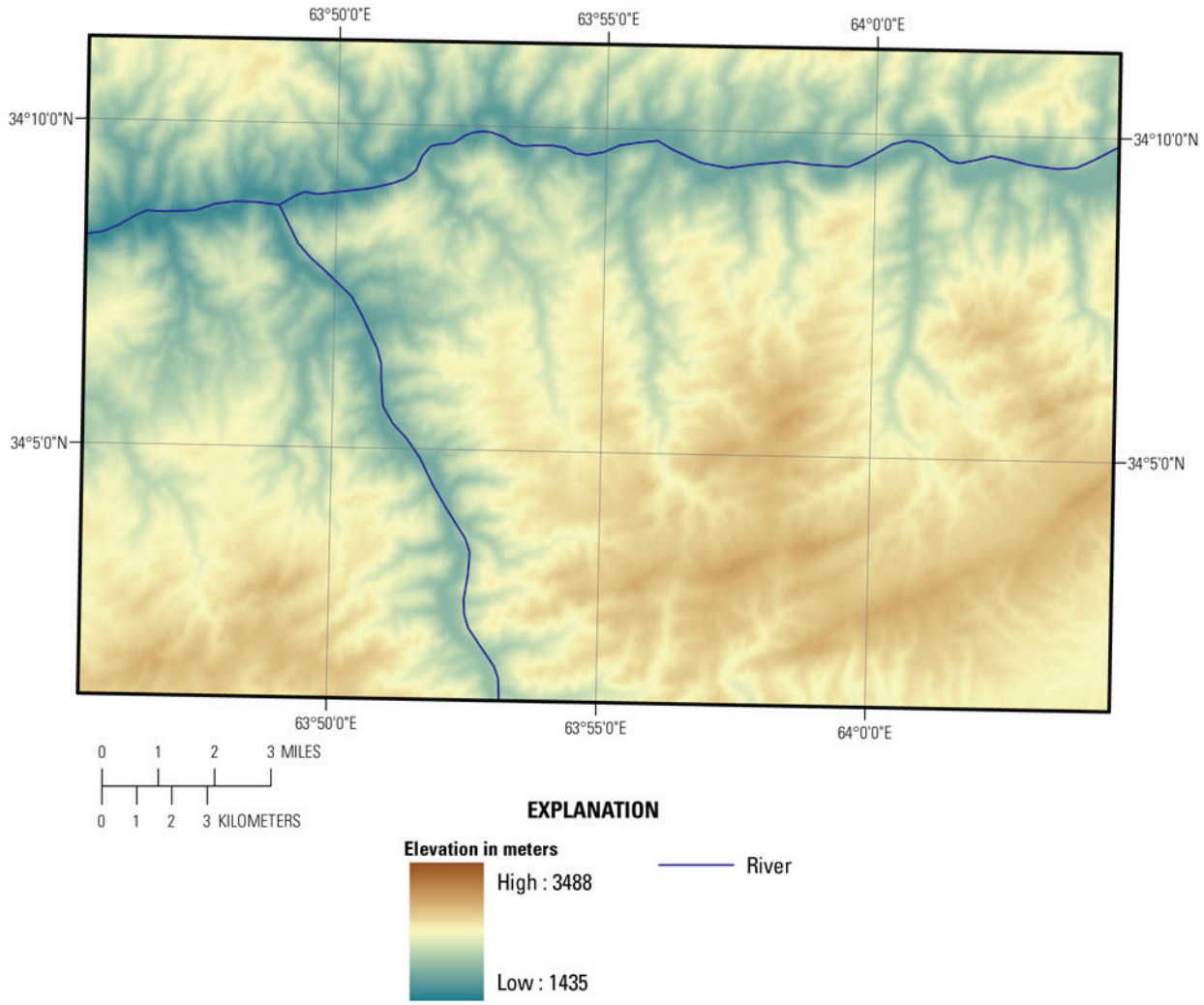

Figure 11B–25. Shaded relief map shows elevation of the Nalbandon District subarea ranges from 1,435 to 3,488 meters. The darker brown tones indicate the higher elevations, and the lower elevations are represented by the blue tones. Two rivers dissect the area; one flows east-west and the other roughly north-south.

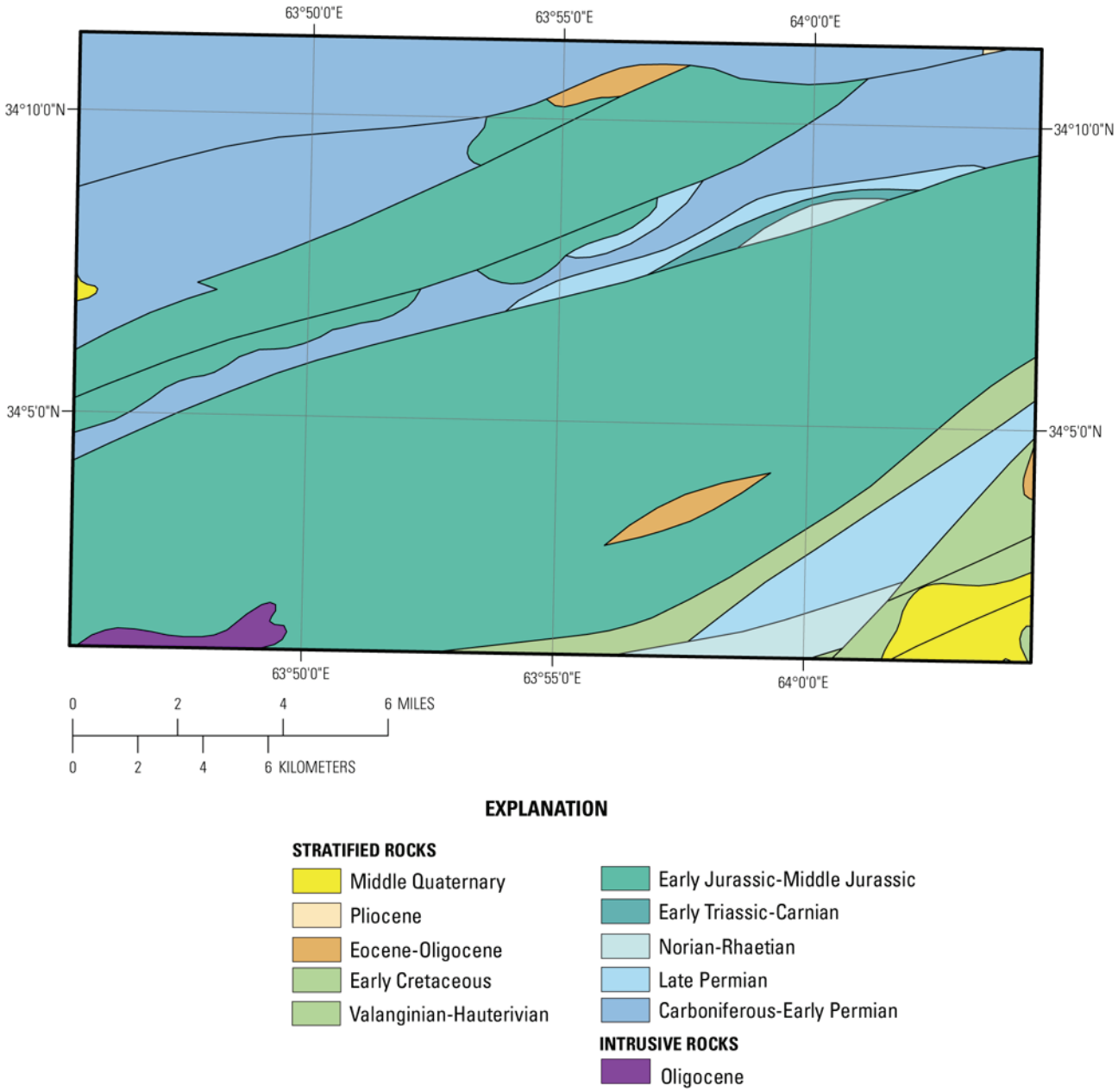

Figure 11B–26. The geologic map of the Nalbandon District subarea of the Nalbandon area of interest is from Doebrich and others (2006).

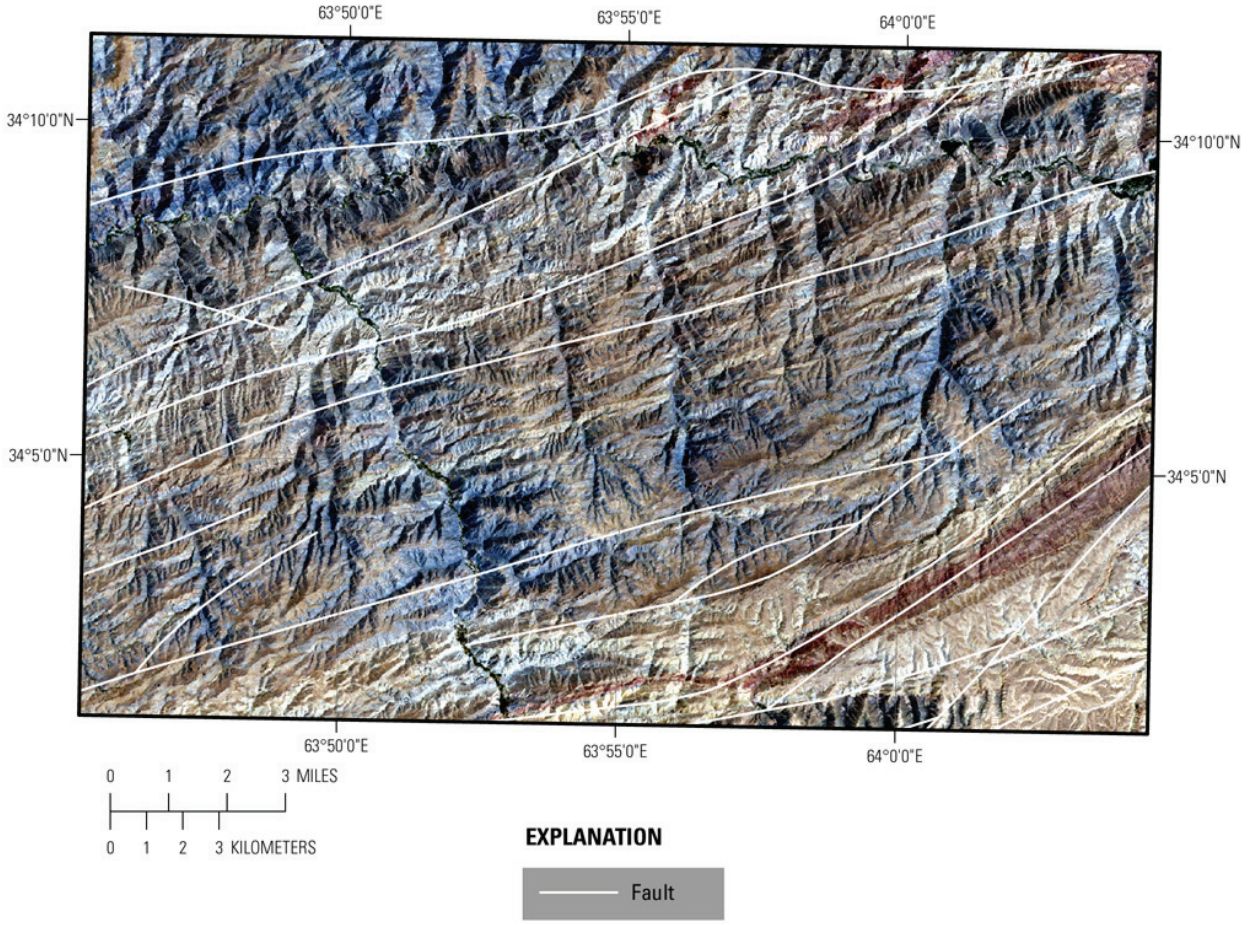

Figure 11B–27. The fault traces (Peters and others, 2007) are placed on a Landsat TM images (Davis, 2007). Color difference in the TM data correlate with different geologic units. The central part of the image (bluish-brown rocks) correlates with the Early–Middle Jurassic age rocks. The dark brown unit in the southeast portion of the image is associated with Early Cretaceous age rocks.

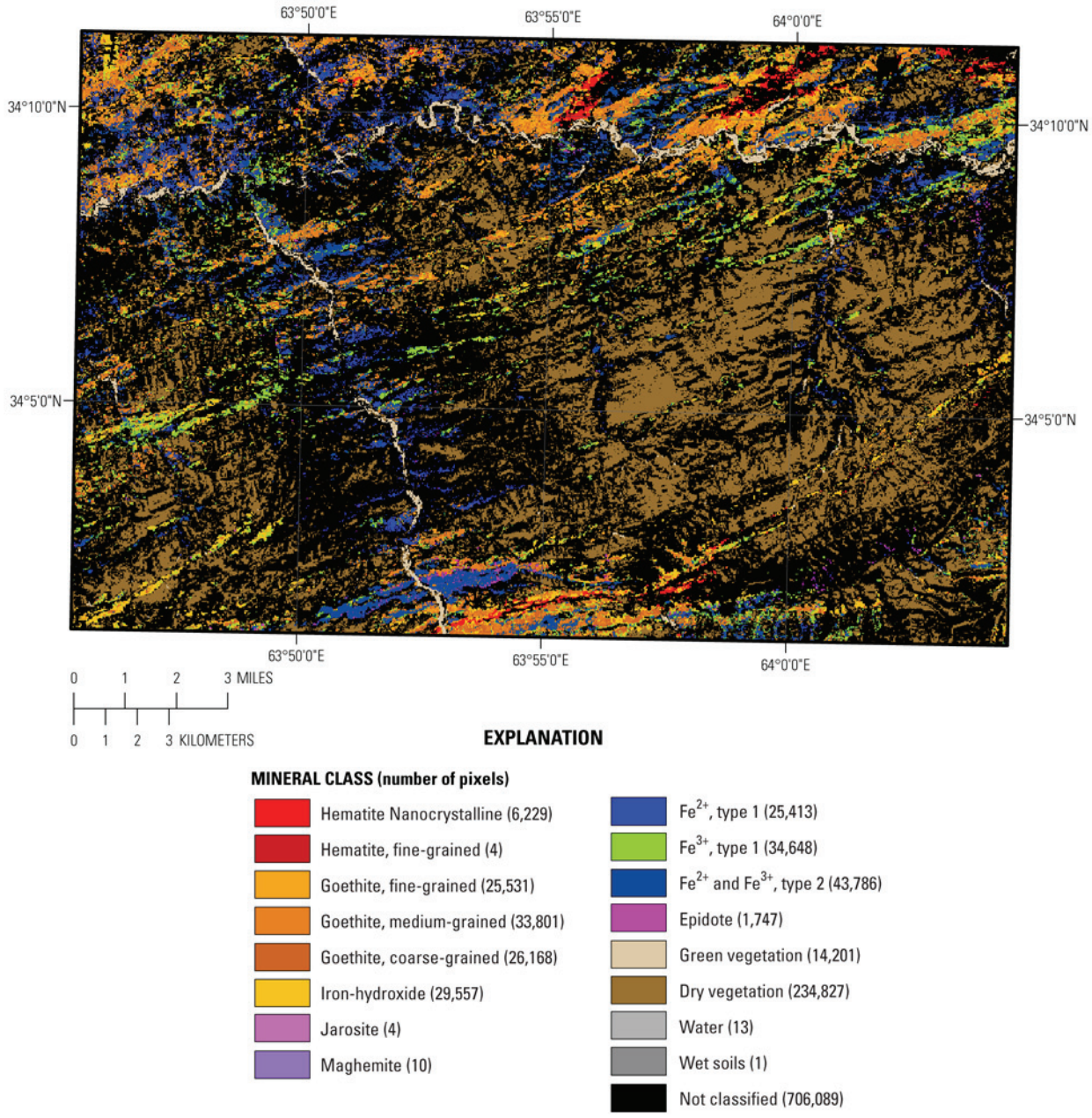

Figure 11B–28. The iron-bearing and other alteration minerals detected in the HyMap data of the Nalbandon District subarea are shown in this image.

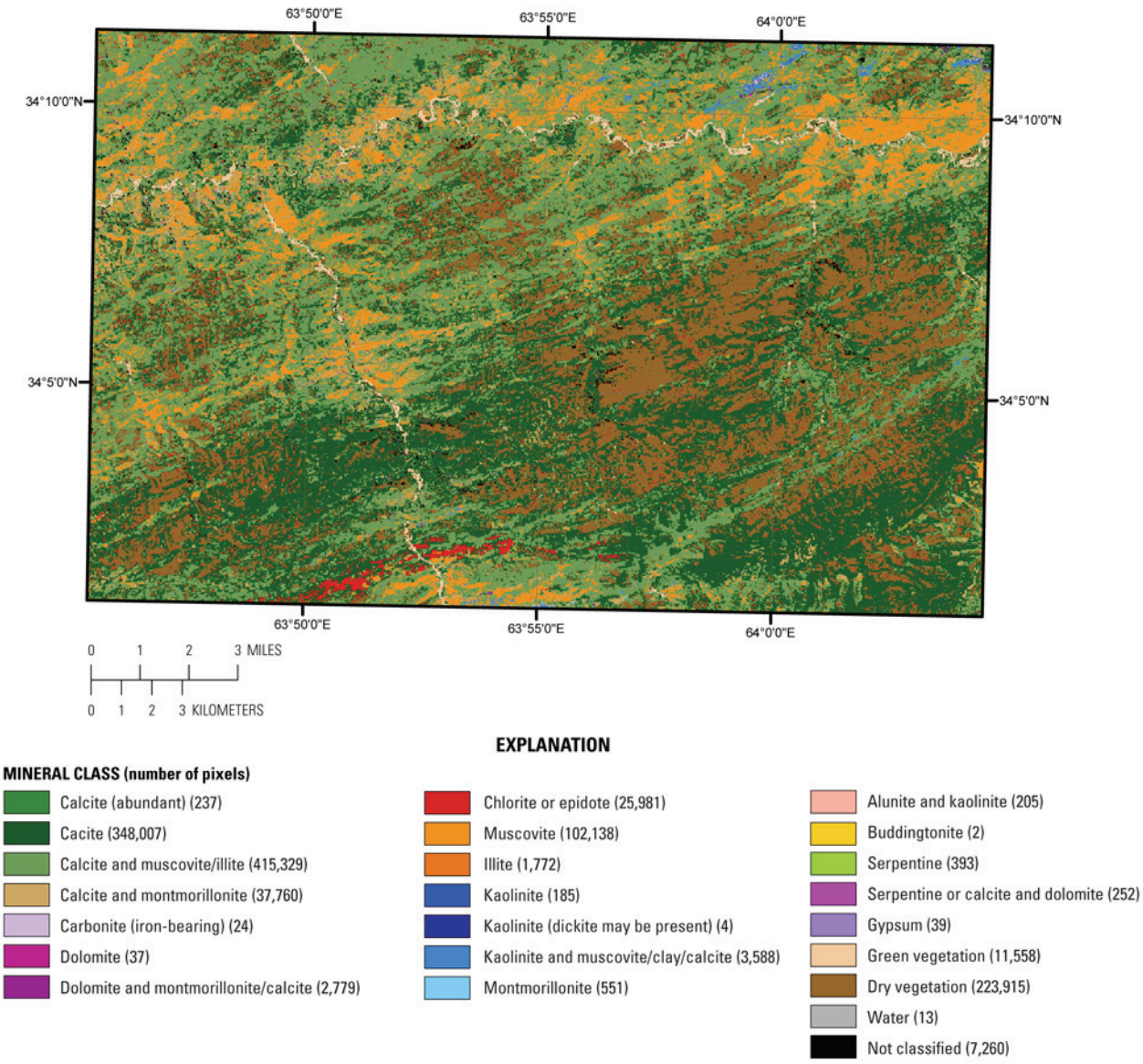

Figure 11B–29. Distribution of clays, carbonates, phyllosilicates, sulfates, altered minerals and other materials for the Nalbandon District subarea of the Nalbandon area of interest using the HyMap data.

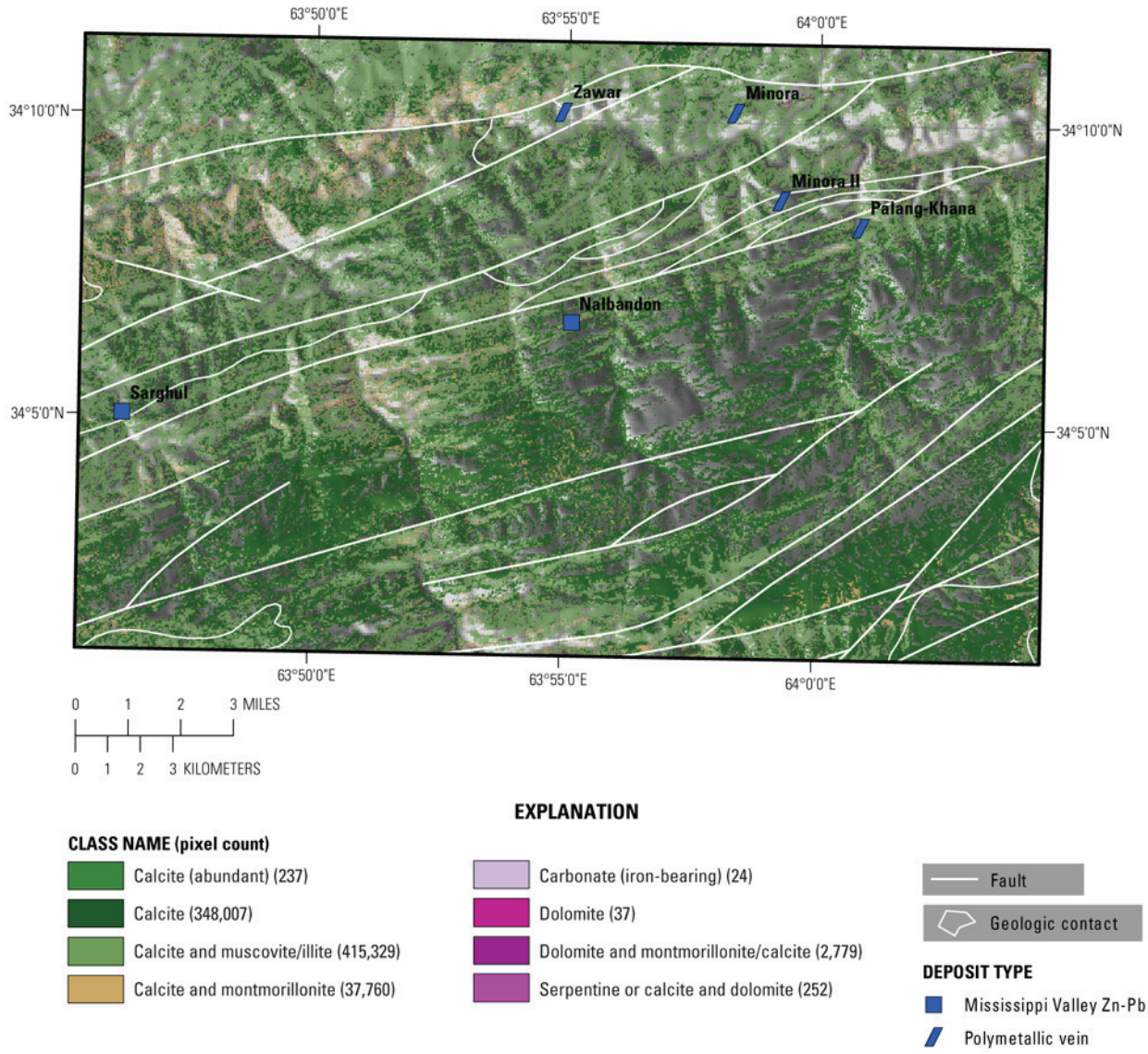

Figure 11B–30. Distribution of carbonate-bearing minerals in the Nalbandon District subarea detected in the HyMap data. Although difficult to see because of the small number of pixels, dolomite and dolomite mixtures are present throughout the area, with small concentrations in the western and north-eastern portion of the mapped area.

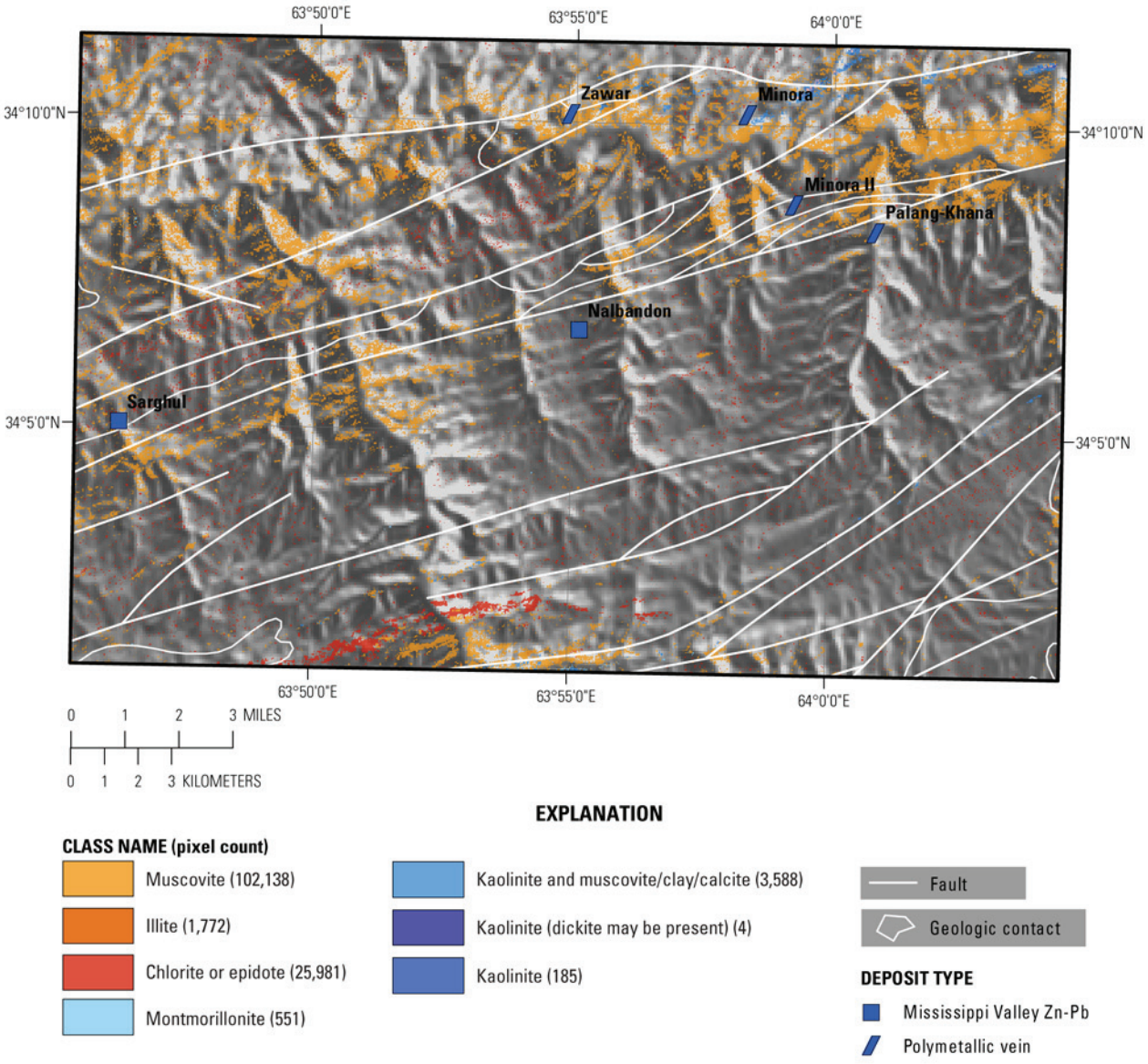

Figure 11B–31. Distribution of clays and micas in the Nalbandon District subarea that were mapped using the HyMap data. The figure shows the occurrence of muscovites and illites and epidote and kaolinite group minerals.

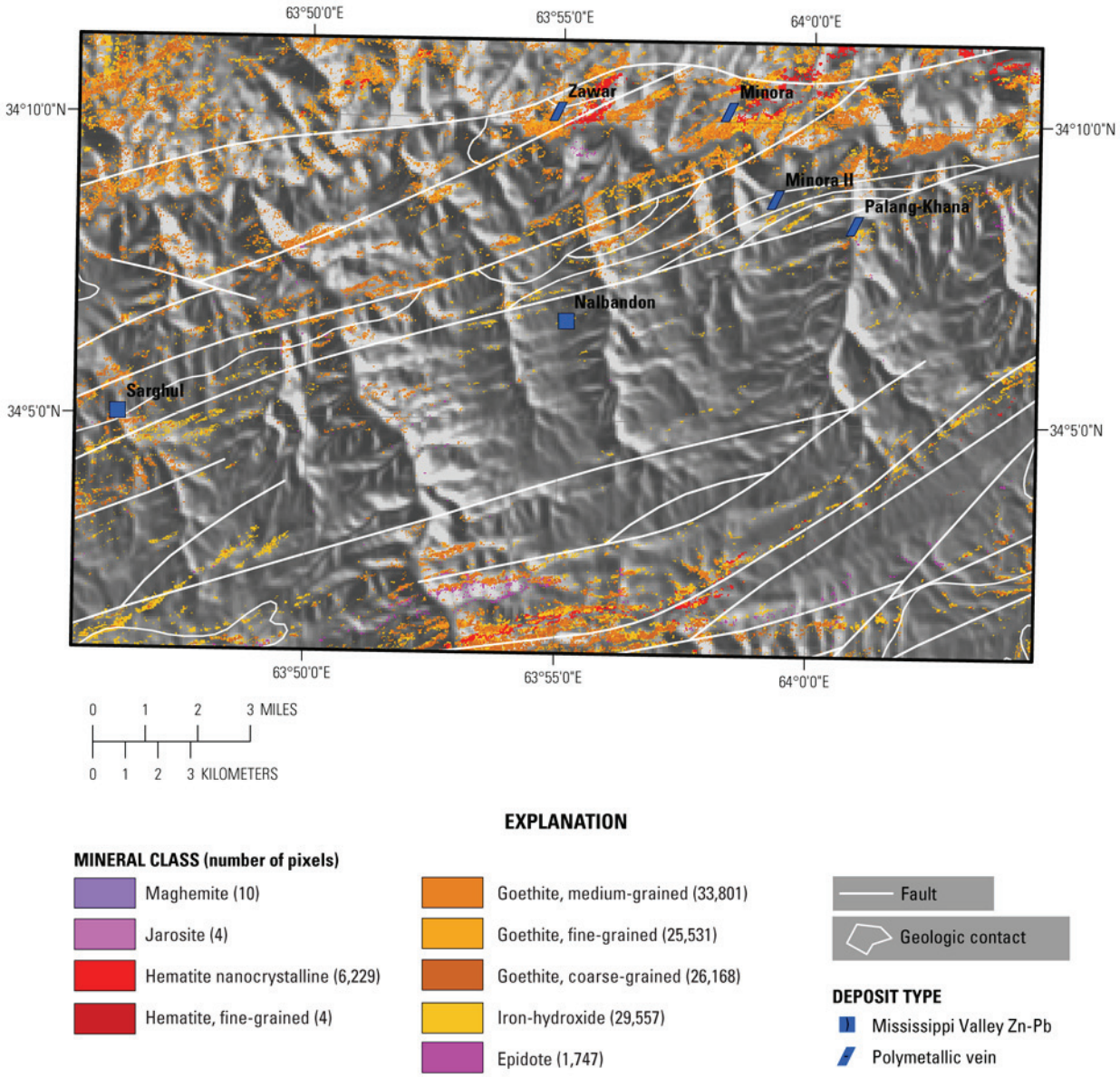

Figure 11B–32. Distribution of iron hydroxides and oxides for the Nalbandon District subarea.

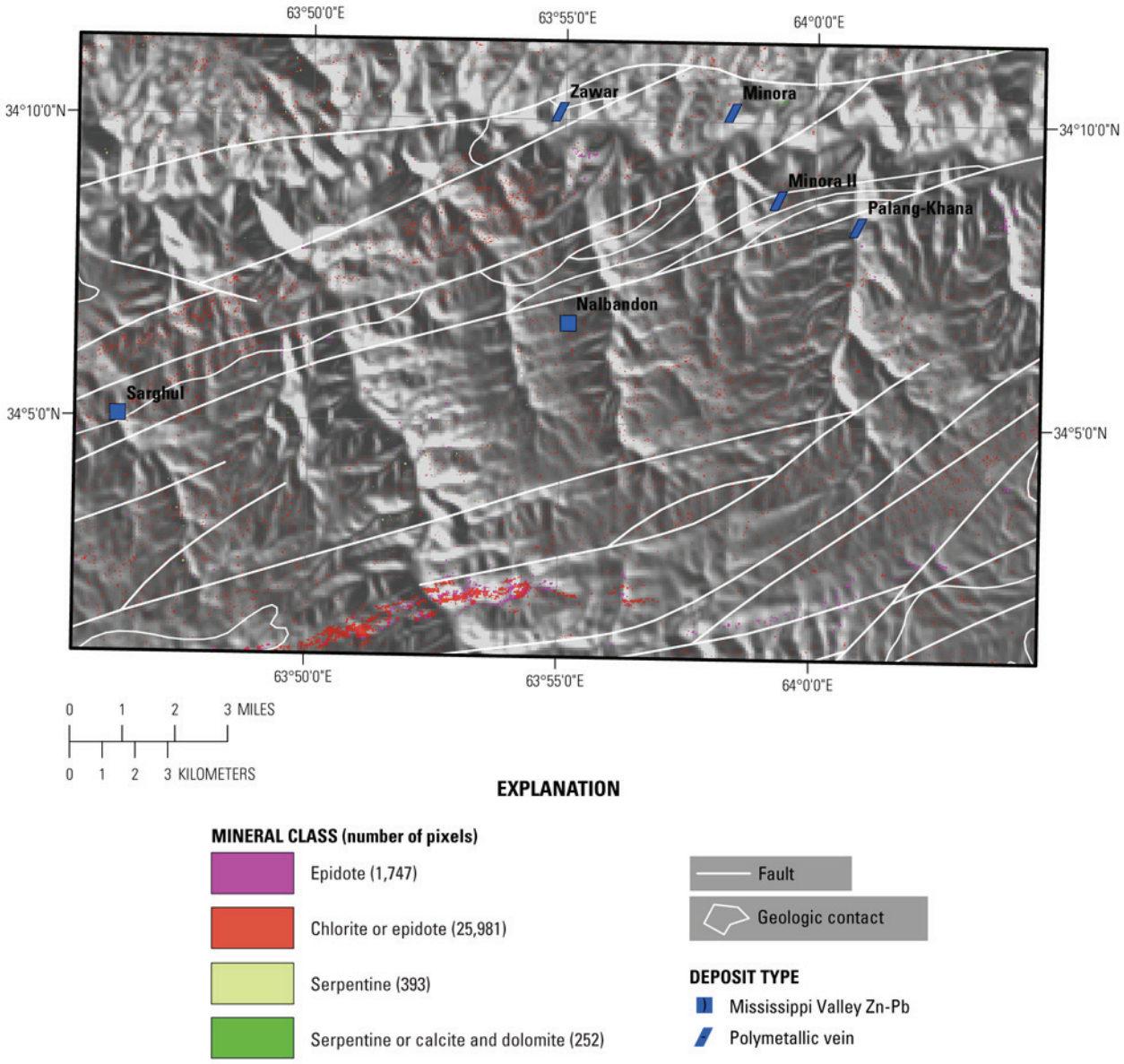

Figure 11B–33. Image showing very limited occurrence and scattered distribution of common secondary minerals detected in the HyMap data for the Nalbandon District subarea of the Nalbandon area of interest.

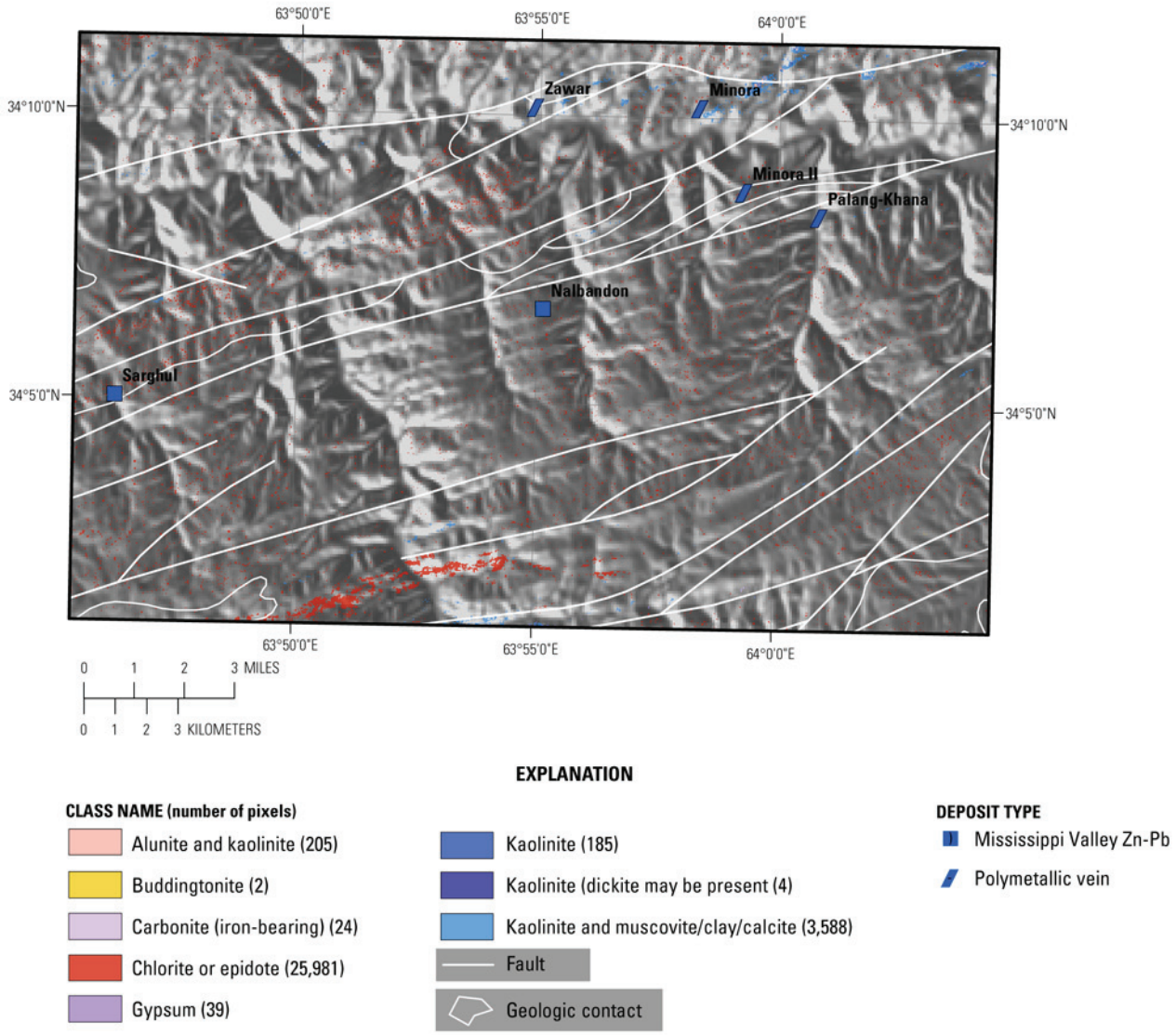

Figure 11B–34. Common alteration materials detected in the HyMap data (fig. 11B–23).

References Cited

Cocks, T., Jenssen, R., Stewart, A., Wilson, I., and Shields, T., 1998, The HyMap airborne hyperspectral sensor—The system, calibration and performance, *in* Schaepman, M., Schlapfer, D., and Itten, K.I., eds., Proceedings of the 1st EARSeL Workshop on Imaging Spectroscopy, 6–8 October 1998, Zurich: Paris, European Association of Remote Sensing Laboratories, p. 37–43.

Davis, P.A., 2007, Landsat ETM+ false-color image mosaics of Afghanistan: U.S. Geological Survey Open-File Report 2007–1029, 22 p. (Also available at *http://pubs.usgs.gov/of/2007/1029/*.)

Doebrich, J.L., and Wahl, R.R., comps., *with contributions by* Doebrich, J.L., Wahl, R.R., Ludington, S.D., Chirico, P.G., Wandrey, C.J., Bohannon, R.G., Orris, G.J., Bliss, J.D., and _____, 2006, Geologic and mineral resource map of Afghanistan: U.S. Geological Survey Open File Report 2006–1038, scale 1:850,000, available at *http://pubs.usgs.gov/of/2006/1038/.*

Dronov, V.I., Kalimulin, S.M., Sborshchikov, I.M., Svezhentsov, V.P., Chistyakov, A.N., Zelensky, E.D., and Cherepov, P.G., 1972, The geology and minerals of North Afghanistan (parts of map sheets 400-II and 500-I, the Kaysar-Hari Rod Interfluve area): [Afghanistan] Department of Geological and Mineral Survey, 44 p.

Hoefen, T.M., Kokaly, R.F., and King, T.V.V., 2010, Calibration of HyMap data covering the country of Afghanistan, *in* Proceedings of the 15th Australasian Remote Sensing and Photogrammetry Conference, Alice Springs, Australia, September 12–17, 2010, p. 409, available at *http://dl.dropbox.com/u/81114/15ARSPC-Proceedings.zip/*.

King, T.V.V., Johnson, M.R., Hoefen, T.M., Kokaly, R.F., and Livo, K.E., 2011, Mapping potential mineral resource anomalies using HyMap data, *in* King, T.V.V., Johnson, M.R., Hubbard, B.E., and Drenth, B.J., eds, Identification of mineral resources in Afghanistan—Detecting and mapping resource anomalies in prioritized areas using geophysical and remote sensing (ASTER and HyMap) data in Afghanistan: U.S. Geological Survey Open-File Report 2011–1229, available at *http://pubs.usgs.gov/of/2011/1229/*.

King, T.V.V., Kokaly, R.F., Hoefen, T.M., Dudek, K. and Livo, K.E., 2011b, Surface materials map of Afghanistan—Iron-bearing minerals and other materials: U.S. Geological Survey Scientific Investigations Map 3152–B.

Kokaly, R.F., King, T.V.V., and Livo, K.E., 2008, Airborne hyperspectral survey of Afghanistan 2007—Flight line planning and HyMap data collection: U.S. Geological Survey Open-File Report 2008–1235, 14 p.

Kokaly, R.F., 2011, PRISM: Processing routines in IDL for spectroscopic measurements—Installation manual and user's guide, version 1.0: U.S. Geological Survey Open-File Report 2011-1155, 512 p.

King, T.V.V., Kokaly, R.F., Hoefen, T.M., Dudek, K. and Livo, K.E., 2011, Surface materials map of Afghanistan—Iron-bearing minerals and other materials: U.S. Geological Survey Scientific Investigations Map 3152–B.

Motza, G., and Silaupa, S, 2010, Geology and mineral resources of Ghor Province Afghanistan: Vilnius, Vilnius University, Cooperation and Democracy Program, 186 p., with appendixes.

Peters, S.G., Ludington, S.D., Orris, G.J., Sutphin, D.M., Bliss, J.D., and Rytuba, J.J., eds., and the U.S. Geological Survey-Afghanistan Ministry of Mines Joint Mineral Resource Assessment Team, 2007, Preliminary non-fuel mineral resource assessment of Afghanistan: U.S. Geological Survey Open-File Report 2007–1214, 810 p., 1 CD–ROM. (Also available at *http://pubs.usgs.gov/of/2007/1214/*.)